Cell trajectory modeling identifies a primitive trophoblast state defined by BCAM enrichment

Matthew Shannon[1,2], Jennet Baltayeva[1,2], Barbara Castellana[1,2], Jasmin Wächter[1,2], Samantha Yoon[1,3], Jenna Treissman[1,2], Hoa T. Le[1,2], Pascal M. Lavoie[1,4], Alexander G. Beristain[1,2]

[1] The British Columbia Children's Hospital Research Institute, Vancouver, Canada.
[2] Department of Obstetrics & Gynecology, The University of British Columbia, Vancouver, Canada.
[3] Department of Surgery, The University of British Columbia, Vancouver, Canada
[4] Department of Pediatrics, The University of British Columbia, Vancouver, Canada.

To whom correspondence should be addressed: Alexander G. Beristain, The British Columbia Children's Hospital Research Institute, The University of British Columbia, Vancouver, British Columbia, Canada. V5Z 4H4. Tel: (604) 875-3573; E-mail: aberista@mail.ubc.ca

Running Title: BCAM in progenitor trophoblasts

Keywords: Placenta, trophoblast, progenitor, single cell RNA-sequencing, differentiation, organoids, basal cell adhesion molecule

Summary Statement: Lineage trajectory modeling identifies multiple human progenitor trophoblast states and defines trophoblast differentiation kinetics, where BCAM-expressing progenitors demonstrate enhanced regenerative ability.

Abbreviations

CTB: Cytotrophoblast
DCT: Distal column trophoblast
DGE: Differential gene expression
EVT: Extravillous trophoblast
FDR: False discovery rate
GO: Gene ontology
HLA-G: Human leukocyte antigen G
Hr: Hour
RT: Room Temperature
IF: Immunofluorescence
scRNA-seq: single cell RNA sequencing
SCT: Syncytiotrophoblast
UMAP: Uniform manifold approximation and projection

ABSTRACT

In early placental development, progenitor cytotrophoblasts (CTBs) differentiate along one of two cellular trajectories: the villous or extravillous pathways. CTBs committed to the villous pathway fuse with neighboring CTBs to form the outer multinucleated syncytiotrophoblast (SCT), while CTBs committed to the extravillous pathway differentiate into invasive extravillous trophoblasts (EVT). Unfortunately, little is known about the processes controlling human CTB progenitor maintenance and differentiation. To address this, we established a single cell RNA sequencing (scRNA-seq) dataset from first trimester placentas to identify cell states important in trophoblast progenitor establishment, renewal, and differentiation. Multiple distinct trophoblast states were identified, representing progenitor CTBs, column CTBs, SCT precursors, and EVT. Lineage trajectory analysis identified a progenitor origin that was reproduced in human trophoblast stem cell organoids. Heightened expression of basal cell adhesion molecule (*BCAM*) defined this primitive state, where BCAM enrichment or gene silencing resulted in enhanced or diminished organoid growth. Together, this work describes at high-resolution trophoblast heterogeneity within the first trimester, resolves gene networks within human CTB progenitors, and identifies BCAM as a primitive progenitor marker and possible regulator.

59 **INTRODUCTION**

60 The placenta is a blastocyst-derived tissue that shares the genetic identity of the developing
61 fetus. Derived from cells of the trophectoderm and extraembryonic mesoderm, the human placenta
62 matures into a functional organ by 10-12 weeks' gestation (GA) (Lee *et al.*, 2016; Chang, Wakeland
63 and Parast, 2018). Through its direct interaction with maternal uterine epithelial, stromal, and immune
64 cells, the placenta coordinates the establishment of the maternal-fetal-interface and serves as a critical
65 barrier important for nutrient-waste exchange between maternal and fetal circulations. Trophectoderm-
66 derived trophoblasts perform many functions of the placenta. These include, but are not limited to the
67 facilitation of nutrient and oxygen transfer between mother and fetus (Burton, Cindrova-Davies and
68 Turco, 2020), the modulation of the maternal immune response towards the semi-allogeneic fetus and
69 placenta (Tilburgs *et al.*, 2015; Turco and Moffett, 2019), and the production of hormones (i.e.
70 chorionic gonadotropin, progesterone, placental lactogen) and other factors required for pregnancy
71 (Fowden *et al.*, 2015).

72 Of all eutherian mammals, the human placenta is the most invasive. Though humans and
73 rodents both share a haemochorial arrangement of trophoblast and uterine tissue, control of uterine
74 surface epithelial and stromal erosion, as well as artery remodeling by trophoblasts during blastocyst
75 implantation and early placental establishment is far more extensive in humans (Turco and Moffett,
76 2019). Importantly, key regulators of trophoblast lineage specification in rodents (i.e. *Cdx2*, *Eomes*,
77 *Esrrb*, and *Sox2*) do not appear to play essential (or identical in the case of *Cdx2*) roles in human
78 trophoblasts (Knöfler *et al.*, 2019). These important differences in human trophoblast biology underlie
79 the need to use human placentas and cell systems for generating fundamental knowledge central to
80 human trophoblast and placental development. While recent advances in regenerative trophoblast
81 culture systems have created the necessary tools required for in-depth cellular and molecular
82 understandings central to trophoblast differentiation (Haider *et al.*, 2018; Okae *et al.*, 2018; Turco *et*
83 *al.*, 2018), to date, few studies have used these platforms to examine at high resolution trophoblast
84 progenitor and/or stem cell dynamics.

85 In humans, two major trophoblast differentiation pathways – villous and extravillous – give rise
86 to all trophoblasts in the fetal-maternal interface (Fig. 1A). In the villous pathway, progenitor
87 cytotrophoblasts (CTBs) fuse with neighboring CTBs to replenish or generate new syncytiotrophoblast
88 (SCT), a multinucleated outer layer of the placenta that is the site of transport of most substances across
89 the placenta. Cells committed to differentiate along the extravillous pathway are predicted to originate
90 from CTB progenitors proximal to anchoring villi (Knöfler *et al.*, 2019), though populations of villous

91 CTB may already be programmed towards extravillous differentiation or may alternatively harbor a
92 level of bi-potency (Chang, Wakeland and Parast, 2018; Lee *et al.*, 2018). Nonetheless, progenitors
93 devoted to this pathway give rise to extravillous trophoblasts (EVTs) that anchor the placenta to the
94 uterine wall (i.e., proximal and distal column CTB). EVTs adopt invasive characteristics hallmarked by
95 interstitial and endovascular EVT subsets, and together facilitate uterine tissue and artery remodeling
96 and modulate maternal immune cell activity (Moffett, Chazara and Colucci, 2017; Pollheimer *et al.*,
97 2018; Papuchova *et al.*, 2020). Defects in trophoblast differentiation along either pathway associate
98 with impaired placental function that may contribute to, or drive the development of aberrant
99 conditions of pregnancy (Jauniaux, Moffett and Burton, 2020).

100 In this study, we combined an in-house-generated single cell RNA-sequencing (scRNA-seq)
101 dataset with a publicly available one (Vento-Tormo *et al.*, 2018) to define trophoblast heterogeneity
102 and differentiation kinetics in the first trimester of pregnancy. Cell trajectory modeling in chorionic
103 villi and regenerative organoid trophoblasts identified a primitive cell origin. Within this upstream
104 progenitor state, we show elevated expression of the gene basal cell adhesion molecule (*BCAM*), where
105 BCAM enrichment or silencing results in enhanced or impaired trophoblast organoid growth,
106 respectively. Together, this work reaffirms and aligns at high-resolution prior knowledge underlying
107 trophoblast heterogeneity and gene signatures specific to stage of trophoblast development. Further,
108 this work identifies BCAM as a conserved cell-matrix adhesion protein in chorionic villous and
109 trophoblast organoid progenitors important for trophoblast stem cell regeneration and growth.

110 **RESULTS**

111 **Single cell transcriptomics resolves trophoblast heterogeneity and cell state dynamics**

112 Single-cell transcriptomic analysis enables the identification of novel cell types and states in a
113 systematic and quantitative manner. Here, we applied the 10X Genomics Chromium platform to
114 sequence the human placental transcriptome at single cell resolution (n=7 placentas), and merged this
115 data with single-cell transcriptomic profiles of human first trimester uterine-placental tissues consisting
116 of 4 placentas and 4 decidual specimens (Vento-Tormo *et al.*, 2018) (Fig. S1). To examine differences
117 in cellular heterogeneity related to stage of development, we grouped individual samples into early (6-7
118 weeks') and late (9-12 weeks') gestational age (GA) groups. Clinical characteristics and sequencing
119 metrics from each patient and sample are summarized (Table S1). 50,790 cells remained after quality
120 control and data pre-processing, and principal component (PC) analysis validated data integration
121 between the two datasets with separation of cells explained by tissue type, not data source (Fig. S1).
122 Cells clustered into 14 cell types and 31 distinct cell states by transcriptomic similarity, and cell cycle
123 phase proportions per cluster informed the level of proliferation in each cell state (Fig. S1). Decidual
124 cells were identified by vimentin expression and decidual immune cells were specifically identified by
125 *PTPRC* transcripts that encode the leukocyte CD45 antigen. Additional markers were used to identify
126 endothelial, stromal, and fibroblastic cell compartments (Fig. S1).

127 For trophoblast identification, cells expressing combinations of trophoblast-related transcripts
128 (i.e. *KRT7*, *EGFR*, *TEAD4*, *TP63*, *TFAP2A*, *TFAP2C*, *GATA2*, *GATA3*, *HLA-G*, *ERVFRD-1*), and
129 lacking mesenchymal- and immune-related transcripts (i.e. *VIM*, *WARS*, *PTPRC*, *DCN*, *CD34*, *CD14*,
130 *CD86*, *CD163*, *NKG7*, *KLRD1*, *HLA-DPA1*, *HLA-DPB1*, *HLA-DRA*, *HLA-DRB1*, *HLA-DRB5*, and
131 *HLA-DQA1*), were subset for further analysis (Fig. S1). Eight trophoblast clusters from 7,798 cells
132 were resolved (Fig. 1B). Within these 8 clusters, we identified four CTB states (CTB1-4; *TEAD4*$^{+}$,
133 *ELF5*$^{+}$), a CTB state expressing SCT-associated genes that we termed precursor syncytiotrophoblast
134 (SCTp; *ERVFRD-1*$^{+}$, *CGB*$^{+}$), two column trophoblast states (cCTB1-2; NOTCH1^{+}, ITGA5^{+}), and a
135 state specific to EVT (EVT; *HLA-G*$^{+}$, *ITGA1*$^{+}$) (Fig. 1C; Table S2). As expected, CTB1-4 showed
136 varying degrees of enrichment for transcription factors associated with trophoblast progenitor/stemness
137 (i.e., *CDX2, TP63*, *ELF5*, *YAP1*), where the CTB3 state showed the greatest level of enrichment of
138 these four genes (Fig. 1C).

139 Column trophoblasts are precursors to EVT, where cells situated within proximal and distal
140 sites of anchoring columns can be molecularly distinguished by expression of NOTCH and integrin
141 genes (Zhou *et al.*, 1997; Haider *et al.*, 2016). To this end, cCTB2 expresses high levels of

142 *NOTCH1*, *SOX9,* and *ITGA2*, the latter of which defines a distinct EVT progenitor population and
143 likely represents a proximal column progenitor (Lee *et al.*, 2018) (Fig. 1C). Compared to cCTB2, cells
144 within the cCTB1 state showed higher levels of *ITGA5*, *NOTCH2*, and *HLA-G*, indicating that this state
145 is developmentally downstream of cCTB2 and cells in this state likely reside within central and distal
146 regions of anchoring columns (Haider *et al.*, 2014) (Fig. 1C). Stratifying cells by phases of the cell
147 cycle showed that cCTB1 column cells are predominately in G_2/M and S phases, while the majority of
148 cCTB2 column cells are in G_1 (Fig. S1). Terminally differentiated EVT and SCTp states are largely G_1
149 cells, as are progenitor CTB1-3 states (Fig S1). This was in contrast to CTB4, where the vast majority
150 of cells are undergoing DNA synthesis and mitosis (Fig. S1), and express hallmark genes of
151 proliferation (i.e. *MKI67*, *CCNA2*), and show enrichment for the transcription factor *TEAD4* (Fig. 1C).
152 Importantly, these distinct trophoblast states largely align with recent single cell transcriptomic
153 characterizations of cells from first trimester pregnancies (Liu *et al.*, 2018; Suryawanshi *et al.*, 2018;
154 Vento-Tormo *et al.*, 2018).

155 Having defined eight trophoblast types/states within first trimester placental tissue, we next
156 examined cell state stability across the first trimester. Relative frequencies of CTB1-4 states increase,
157 whereas proportions of cCTB and EVT states decrease from early (6-7 weeks') to late (9-12 weeks')
158 gestation (Fig. 1D). Notably, an almost 5-fold reduction in the proportion of EVT (19% to 4%) is
159 observed (Fig. 1D), suggesting that villous development and branching contribute to the increase in
160 CTB frequency. Unexpectedly, and unlike CTB1-4, frequencies in SCTp remained relatively constant
161 (8-9%) (Fig. 1D), though, as with all trophoblast proportions, accuracy is highly dependent on
162 minimizing biases in single cell dissociation and cell capture pipelines prior to barcoding and
163 sequencing. Together, these findings define unique states of trophoblasts in the first trimester placenta
164 and highlight how proportions of these states change between the early and late first trimester, a
165 developmental window during which the human placenta becomes fully functional.

166

167 **Single cell trajectory modeling identifies a CTB origin**

168 RNA velocity, the time derivative of the gene expression state, can be used to predict the future
169 transcriptional state of a cell. RNA velocity analysis in combination with single-cell trajectory analyses
170 provides us with insights into the transcriptional dynamics of developing cells and enables high-
171 resolution lineage pathway ordering. By applying scVelo to our dataset to refine progenitor and cell
172 end-point relationships, we identified an origin that overlapped with CTB2; this predicted origin was

173 also proximal to the CTB3 state, indicating that these two states contain a proportionally high content
174 of primitive trophoblasts (Fig. 2A). Two paths were identified extending from this origin towards the
175 EVT state and one path developing from the origin towards the SCTp state. As well, we found an
176 additional differentiation trajectory, extending from CTB2 into CTB3, representing possible CTB
177 progenitor reserves or progenitor states in transition (Fig. 2A). When shown in a 3D perspective, a
178 linkage between CTB3 and CTB4 becomes evident that is not obvious in 2D clustering, indicating that
179 the CTB2 state can transition to the proliferative CTB4 state via multiple cell pathways (Fig. S2).
180 Monocle3 pseudotime ordering was also applied to increase confidence in trophoblast hierarchical
181 ordering. Similar to RNA velocity, CTB2 was identified as a state aligning to the origin (though CTB1
182 also showed partial overlap); increased complexity is observed as CTBs progress along one of two
183 trajectories that lead to either EVT or SCT end-point states (Fig. S3). Specifically, Monocle3 ordering
184 revealed a looped trajectory within CTB2 that exits towards CTB3, SCTp, and EVT states (Fig. S3).

185 We next compared these refined trajectories with expression patterns of known CTB
186 progenitor/stem cell genes *CDX2, TEAD4, YAP1, TP63, ELF5,* and *EPCAM*. Predominant expression
187 of *ELF5, TEAD4,* and *YAP1* was observed in all CTB states, while expression of the CTB stem cell
188 transcription factor *CDX2* showed predominant levels in cells in CTB1 and CTB3, and to a lesser
189 extent CTB2 and CTB4 (Fig. 2B). Average *TP63* expression was highest in CTB3, though a greater
190 proportion of cells within CTB2 expressed *TP63* compared to other CTB states, and *EPCAM* showed
191 greatest enrichment within the CTB1 and CTB4 (Fig. 2B). Because the scVelo-predicted origin aligned
192 closely to CTB2 and CTB3, we examined genes both shared and enriched in each of these states (Fig.
193 2C). Twenty-four genes were shown to overlap between CTB2 and CTB3, including *EGFR, IGF2,* and
194 *FBLN1* (Fig. 2C; Table S3). 249 genes showed enrichment in CTB3, and of these many associate with
195 trophoblast stem cell and regenerative properties (i.e., *YAP1, TP63*), Wnt signaling (*LRP5*), and cell-
196 matrix interactions (*MMP14, MMP15, ITGA6, LAMA5, LAMB1*) (Fig. 2C). The CTB2 state showed
197 enrichment for 251 genes, including the Wnt ligand, *WNT7A*, the laminin receptor basal cell adhesion
198 molecule (*BCAM*), and the transcriptional modulators *TFAP2A* and *CITED2* (Fig. 2C). Expression
199 levels of the top twenty-five CTB2-enriched genes (FDR ranked) plotted by cell state over a simple
200 branched pseudotime [as performed previously using Monocle 2 in (Vento-Tormo *et al.*, 2018;
201 Treissman *et al.*, 2020)] showed consistent enrichment of all genes to the CTB origin (Fig. 2D).
202 Notably, some genes (e.g., *BCAM, IFI6*) show a consistent down-regulation along the SCT and EVT
203 trajectories, while others (e.g., *DUSP9, GSTA3, VAMP8*) show transient decreases followed by
204 increases in gene levels approaching SCT or EVT trajectory endpoints (Fig. 2D). scVelo-alignment of

205 *BCAM,* a gene encoding a cell-ECM laminin receptor and one of the most enriched genes within the
206 CTB2 state (Table S2), shows that *BCAM* levels are highest within the predicted CTB origin, and
207 gradually decrease as CTBs differentiate into SCTp or cCTB/EVT (Fig. 2E). Taken together, we have
208 identified a primitive CTB state within the first trimester placenta that shows molecular features
209 consistent with that of putative CTB stem cells. We also identify multiple genes aligning with this
210 origin, many of which have not being described in trophoblast progenitor biology, including the gene
211 *BCAM*.

212

213 **Trophoblast stem cells recapitulate scRNA-seq-informed CTB heterogeneity and hierarchy**

214 Recently described regenerative human trophoblast models provide an improved method for
215 studying trophoblast differentiation *in vitro* (Okae *et al.*, 2018). Three-dimensional organoid cultures
216 established from human trophoblast stem cell lines (hTSCs) also reproduce molecular features
217 underlying CTB maintenance and differentiation (Saha *et al.*, 2020). To examine the reproducibility of
218 trophoblast-intrinsic differentiation programs defined by scRNA-seq analysis of chorionic villous
219 tissues, we subjected three hTSC lines to scRNA-seq analysis prior to and following EVT
220 differentiation. hTSC organoids (CT27, CT29, and CT30 CTB lines) were cultured for 7 days in
221 regenerative Wnt^+ (containing the Wnt potentiators R-spondin and CHIR99021) and EVT-
222 differentiating Wnt^- (lacking R-spondin and CHIR99021) media, respectively, prior to single cell
223 workflow. To confirm the intactness of our system, a separate cohort of hTSC organoids were cultured
224 over 21 days in these media and differentiation was assessed by light microscopy, flow cytometry, and
225 qPCR analysis. hTSC-derived organoids cultured in regenerative media established large spherical
226 colonies characterized in part by elevated expression of the CTB progenitor genes *TEAD4* and *ITGA6*
227 (Fig. 3A, 3B). Moreover, expression of surface MHC-I (HLA-A, -B, -C) by flow cytometry did not
228 detect these MHC-I ligands in undifferentiated cultures (Fig. 3C). Comparatively, hTSC organoids
229 cultured in EVT differentiating Wnt^- media showed characteristic cellular extensions from the organoid
230 body (Fig. 3A), as well as a marked decrease in levels of *TEAD4* mRNA (Fig. 3B). As expected, both
231 immature (*ITGA5*, *NOTCH1*) and mature (*NOTCH2*, *HLA-G*) EVT marker genes, as well as HLA-C
232 and HLA-G surface expression increased along the EVT differentiation timeline (Fig. 3B, 3C).
233 Syncytial formation occurs in both regenerative Wnt^+ and EVT Wnt^- conditions, and this was reflected
234 at the gene level were *CGB* and *CSH1* levels markedly increased over 21 days (Fig 3C). Together,
235 these data indicate that the 3D organoid model to study CTB regeneration and differentiation is intact.

236 Regenerative and EVT-differentiated hTSC organoid cells were then used to generate single
237 cell cDNA libraries following 10X Genomics Chromium workflow. Combining single cell
238 transcriptomic data from CT27, CT29, and CT30 organoids resolved 7 distinct cell states; three CTB
239 (CTB1-3), a precursor to syncytiotrophoblast (SCTp), a putative column/EVT progenitor (cCTB), and
240 two EVT-like states (EVT1, EVT2) (Fig. 3D). Hallmark gene markers of trophoblast-lineage (*TFAP2A,*
241 *TFAP2C*), progenitor CTB (*TEAD4, YAP1, TP63, ITGA6, ELF5*), syncytiotrophoblast (*ERVFRD-1,*
242 *ERVV-1, SDC1*), immature (*ITGA5, ITGA2, NOTCH1*) and mature EVT (*ITGA1, NOTCH2, HLA-G*),
243 as well as gene markers of proliferation (*MKI67, CCNA2*) are shown corresponding to individual cell
244 states (Fig. 3D; Table S2). CTB1-3 shared moderate overlap in gene expression, though CTB1
245 distinctly co-expressed proliferative and progenitor genes (Fig. 3D). While CTB2 and CTB3 also
246 expressed progenitor genes, levels were comparatively lower than levels in CTB1 (Fig. 3D). The
247 putative column/EVT progenitor state, cCTB, uniquely expressed *ITGA2*, *SOX9*, and the immature
248 EVT marker *NOTCH1*; at the gene level, this unique state resembles the EVT progenitor population
249 described by Lee *et al.* (2018) (Fig. 3D). States resembling terminally differentiated cell types showed
250 strong enrichment for syncytiotrophoblast- and EVT-associated genes, with EVT1 showing the highest
251 levels of *HLA-G* and *NOTCH2* (Fig. 3D).

252 When scRNA-seq data for hTSC organoids are plotted individually, overall cell state
253 complexity reduces from 7 to 5 states (Fig. 3E). Intercomparison of hTSC lines showed notable
254 variances in cell heterogeneity (Fig. 3E). While defined SCTp and EVT endpoint states are evident in
255 all three lines, variances defined by gene expression in CTB and cCTB states suggest that the hTSC
256 lines have distinct cell differentiation kinetics or pathways unique to themselves (Fig. 3E). Nonetheless,
257 within each hTSC organoid, scVelo revealed a common CTB origin aligning to CTB1 (Fig. 3E).
258 Similar to scVelo modeling in chorionic villi, 3D rendering of scVelo trajectories in organoids
259 highlight multiple pathways extending from CTB1 to EVT, while a more direct single path is shown
260 for SCTp establishment extending from CTB3 (Fig. S4). Examining gene signatures within these
261 origins showed consistent enrichment of the trophoblast progenitor genes *TP63* and *YAP1*. However,
262 we did see differences in levels of *ELF5* between hTSC lines. Specifically, *ELF5* was enriched in
263 CTB2 in the CT27 and CT29 hTSC lines but aligned more with the origin and the CTB1 state in the
264 CT30 hTSC line (Fig. 3E). Similar differences were observed for the proliferative gene markers *MKI67*
265 and *CCNA2*, where levels were enriched within CTB1 of CT27 and CT30 but aligned more specifically
266 to CTB2 in CT29 (Fig. 3E). When averaged across all hTSC lines, however, we observed consistent
267 expression of *ELF5*, *BCAM*, *MKI67*, and *CNNA2* within the CTB1 state that overlapped with the

268 predicted origin (Fig. 3D). Comparison of transcriptional signatures between the scVelo-determined
269 origins in CTB from chorionic villi and in hTSC organoids highlights that there is considerable overlap
270 between CTB2 (*in vivo*) and CTB1 (*in vitro*), as well as notable differences (Fig. 3F; Table S3). 481
271 genes are shared, whereas 1430 and 1406 genes are enriched within the origin states of chorionic villi
272 and organoids, respectively (Fig 3F). A differential gene expression analysis between CTB2 (villi) and
273 CTB1 (organoids) revealed 13,364 differentially expressed genes (Fig. 3G; Table S4). Pathway
274 analysis of these signatures shows that organoid progenitors have enrichment of pathways underlying
275 cell division and microtubule assembly, indicative of a pro-proliferative state, while villous progenitors
276 showed enrichment of genes related to respiration, mitochondrial function, and inorganic transporter
277 activity (Fig. 3H). Consistent with data from primitive CTB in chorionic villi, *BCAM* was shown to be
278 one of the most highly expressed and FDR-ranked genes shared between organoid CTB1 and villous
279 CTB2 states (Table S3), and also highly overlapped with the scVelo-predicted origin (Fig. 3I, 3J).
280 These data show that molecular programs are largely conserved in hTSC organoids, that similarities in
281 overall trophoblast heterogeneity are maintained, and that cell adhesion molecule *BCAM* is also a
282 shared marker of regenerative CTB in chorionic villous and hTSC organoids.

283

284 **BCAM confers increased CTB regenerative potential**

285 To our knowledge, BCAM localization within the human placenta has never been reported. To
286 this end, we probed early (6.3 week) and late (11.2 week) first trimester placental villi specimens with
287 BCAM antibody (Fig. 4A). A specific and strong BCAM signal was observed in CTB of both
288 developmental time-points, and serial sections stained with keratin-7 (KRT7) and HLA-G showed that
289 BCAM was present within proximal column cells, though the intensity of the signal was less than in
290 villous CTB (Fig. 4A). Serial sections of chorionic villi stained with KRT7 and hCG clearly showed
291 that BCAM is absent from the syncytiotrophoblast outer layer (Fig. 4A). Consistent with this, in hTSC-
292 derived organoids cultured in regenerative conditions, BCAM signal was specific to the outer CTB
293 layer and absent within the inner hCG^{+} syncytium (Fig. 4B). Dual labeling with BCAM and Ki67
294 antibody showed that $BCAM^{+}$ CTB also co-express the proliferation marker (Fig. 4B).

295 To test the regenerative potential of BCAM-expressing cells, $BCAM^{hi}$ and $BCAM^{lo}$ CTBs were
296 sorted from CT29 hTSC organoids, seeded at a density of 125 cells/μl within Matrigel domes, and
297 cultured over 11 days (Fig. 4C, 4D). While the colony take-rate did not differ between $BCAM^{hi}$ and
298 $BCAM^{lo}$ CTB organoids (Fig. S5), the colony size of $BCAM^{hi}$ organoids appeared to be larger by day

7, with BCAM^{hi} -derived colonies being significantly larger than BCAM^{lo} -derived colonies on days 9-11 in culture (Fig. 4D, 4E). Flow cytometry assessment of day 11 BCAM^{hi} - and BCAM^{lo} -derived organoids showed that >90% of BCAM^{hi}-sorted cells retained high levels of BCAM surface expression (Fig. 4F), while the frequency of CTBs expressing high levels of BCAM in BCAM^{lo}-sorted cells was 70%, suggesting that the BCAM phenotype is dynamic. While a minor EGFR^{lo} population was detected in endpoint organoids from BCAM^{hi}-sorted CTBs, a significant expansion in this population was evident in organoids derived from BCAM^{lo}-sorted CTBs, suggesting that BCAM^{lo} CTB do not retain regenerative properties as robustly as BCAM^{hi} CTB (Fig. 4F). Comparing differentially expressed genes between CTB expressing high or low levels of *BCAM* in organoid scRNA-seq data showed that elevated *BCAM* levels associate with higher levels of the paternally imprinted transcription factor *PEG10*, and the stem cell renewal genes *EPCAM* and *HMGB3* (Nemeth, Kirby and Bodine, 2006) (Fig. 4G).

To specifically examine if BCAM plays a functional role in promoting trophoblast organoid growth, two *BCAM*-targeting siRNAs were transfected into CT29 hTSCs prior to and during organoid development, and organoid growth was monitored over 7 days. Non-transfected and non-silencing siRNA-transfected (siCTRL) CT29 hTSCs served as controls. siRNA-directed knockdown of BCAM showed a 40-60% reduction in BCAM protein levels at days 3 (mid) and 7 (endpoint) of culture (Fig. 5A, 5B). While non-transfected and siCTRL organoids formed large and robust colonies, BCAM silencing led to a consistent reduction in organoid colony size (Fig. 5C). Whereas control hTSCs formed greater frequencies of medium (2.0 - 4.9 x10^4 μm^2) and large (> 5.0 x10^4 μm^2) organoids, BCAM silenced hTSCs formed greater frequencies of small (< 2.0 x10^4 μm^2) colonies (Fig. 5D). Similar to our observation that BCAM^{lo} sorted CTB showed an enhanced expansion of a EGFR^{lo} population, BCAM silencing in organoids led to a modest but significant increase in the frequency of EGFR^{lo} trophoblasts, suggesting that a reduction in BCAM may result in greater plasticity or accelerated differentiation (Fig. 5E). We also examined if BCAM impacts cell cycle kinetics, and by assessing DNA content using flow cytometry we show that BCAM silencing results in a modest, but not significant, increase in the proportion of trophoblasts in G_2 phase, and a reciprocal, but not significant, decrease in the frequency of cells in S phase (Fig. 5F). Similarly in day 7 endpoint organoids, BCAM-silencing showed a reduction in the proportion of BrdU$^+$ cells compared to frequencies in non-silencing controls, though this too did not reach statistical significance, likely attributed to variability in organoid growth and BrdU assessment of 3D cultures by IF (Fig. 5G).

331 **DISCUSSION**

332 Here we applied single cell RNA sequencing of human placentas at two gestational age ranges
333 within the first trimester to further our understanding of human trophoblast development. In doing this,
334 we provide here novel transcriptomic data from 7,798 human trophoblasts, resolve the first trimester
335 trophoblast landscape at increased resolution, and clarify how trophoblast heterogeneity changes during
336 the first trimester. Using state-of-the-art single cell lineage trajectory tools, we trace back the lineage
337 commitments made by developing CTBs to identify a trophoblast progenitor origin marked by
338 increased expression of the cell surface glycoprotein BCAM. BCAM's association with the predicted
339 CTB origin highlights an additional utility of using BCAM as a new cell surface progenitor marker for
340 future studies identifying and defining CTB progenitors.

341 Previous studies have explored the placental transcriptome at single cell resolution (Liu *et al.*,
342 2018; Suryawanshi *et al.*, 2018; Vento-Tormo *et al.*, 2018). While these studies have contributed
343 important insight into placental cell heterogeneity, a strict focus on understanding CTB hierarchy and
344 gene pathways underlying CTB regeneration and commitment to EVT or SCT was not a focus of these
345 studies. Our study identifies four unique CTB states that are distinguishable by state of metabolism
346 (protein translation, CTB1; mitochondrial regulation, CTB3), cell cycle (CTB4), and molecular
347 readouts of respiration and transporter activity (CTB2). Concurrent single cell analyses using hTSC-
348 derived organoids identifies similar cell states found in vivo, though differences in the number of cell
349 state clusters and specific genes in organoids derived from unique hTSC lines does suggest CTB
350 clusters may represent snap-shots of transient cell states captured during CTB maintenance and
351 differentiation, and are not specific cell types *per se*.

352 Using scVelo and Monocle3, we identified a CTB origin that likely represents a primitive stem
353 cell-like niche. CTB2 was identified by both scVelo and Monocle3 trajectory modeling tools as the
354 CTB state overlapping with this predicted origin. We were initially surprised to see the predicted origin
355 did not directly align with CTB3, as this state showed robust levels of many classical CTB progenitor
356 genes like *YAP1, TEAD4*, and *TP63,* where by comparison CTB2 expressed lower levels of these
357 known progenitor genes. However, CTB2 did show enrichment for some important CTB-associated
358 genes like *SPINT1* (Walentin *et al.*, 2015), and further showed elevated levels for the Wnt ligand
359 *WNT7A* and other Wnt-modifying factors like *GPC3*, *DAB2*, and *DACT2* (Jiang, He and Howe, 2012;
360 Capurro *et al.*, 2014; Wang *et al.*, 2015), suggesting that this state is responsive to WNT signaling, an
361 important feature underlying *in vitro* CTB progenitor maintenance (Okae *et al.*, 2018).

362 Comparisons between our placental tissue sequencing data and our trophoblast organoid

363 sequencing data demonstrate similarities in general CTB, SCT and EVT function, but also subtle
364 differences between the different states of CTB found in each stem cell derived organoid condition and
365 our tissue CTBs. Comparison of the CTB progenitor niche identified in both the organoid and tissue
366 datasets identifies the common transcription factors *YAP1*, *SPINT2*, *PEG10*, and *MSI1* as well as
367 consistent upregulation of *BCAM*, supporting identification of BCAM as a CTB progenitor marker.
368 Interestingly, quantification of mRNA levels of known CTB related genes (*TEAD4* and *ITGA6*) as well
369 as SCT (*CGB* and *CSH1*) and EVT related genes (*ITGA5*, *NOTCH1*, *NOTCH2*, and *HLA-G*) on days 0,
370 11, and 21 of differentiation indicate that hTSC specific organoid colonies show different rates of
371 differentiation or capacities to differentiate. Our EVT-differentiated organoid transcriptomes were
372 sequenced on day 7 of differentiation, indicating that the differences we are observing may in part be
373 due to groups of organoid colonies being at a different stages of differentiation, with CT29 derived
374 organoids showing the most rapid capacity for EVT differentiation, followed by CT30 and CT27.
375 These differences in differentiation kinetics or capacities should be taken into consideration by
376 researchers aiming to use these regenerative trophoblast lines for future research.

377 Consistent between chorionic villous and organoid datasets is the identification of two CTB
378 progenitor states in the first trimester placenta, one representing a CTB origin state marked by elevated
379 *BCAM*, and one representing a more specified bipotent EVT progenitor cell state, marked by *ITGA2*
380 and *NOTCH1*. In 8-9 week GA placental villi, ITGA2 is specific to proximal cells within anchoring
381 placental villi near the basement membrane (Lee *et al.*, 2018). It is thought that as chorionic villi
382 develop, trophoblast progenitors within close proximity to uterine stroma adopt a unique gene
383 expression profile that predisposes their differentiation along the extravillous pathway. We show that
384 the transcriptome of *ITGA2*$^{+}$ putative column progenitors express EVT-associated genes such as
385 *NOTCH1* and *ITGA5,* as well as the CTB/progenitor-associated genes *GATA3* and *ELF5*. ITGA2^{+}
386 cCTBs are described as having a level of bipotency. Analyses using scVelo suggests
387 *ITGA2*$^{+}$column/EVT progenitors descend from the *BCAM*$^{+}$ CTB progenitor origin and are maintained
388 as a reserve progenitor population, though whether this state represents a bipotent CTB state will need
389 to be fully examined, but nonetheless our analyses demonstrate a detailed molecular signature for this
390 interesting EVT progenitor state.

391 We identify *BCAM* as a gene expressed by CTB progenitors, where its expression is particularly
392 elevated in the most upstream CTB states. BCAM interacts predominantly with its ligand *LAMA5*, a
393 component of the laminin-511 heterotrimers found within the placental extracellular matrix (Zen *et al.*,
394 1999; Kikkawa *et al.*, 2013). BCAM is an antigen upregulated in ovarian carcinoma, and facilitates

395 tumor migration by competing for laminin binding with integrins (Kannan *et al.*, 2015; Guadall *et al.*,
396 2019). Here, we show that flow-cytometry enrichment of BCAM in CTBs significantly potentiates
397 CTB organoid growth. Interestingly, no differences were observed in the capacity of BCAM^{hi} or
398 BCAM^{lo} CTBs to form organoid colonies from single cells, suggesting that BCAM^{hi} CTB may not
399 have intrinsically greater stem-like properties over BCAM^{lo} CTB. Rather, BCAM may enhance
400 organoid growth by potentiating survival signals induced by cell-ECM engagement, or by
401 initiating/driving CTB proliferation pathways. However, we show that genes associated with stem cell
402 regeneration are elevated in BCAM^{hi} hTSC-derived organoids as compared to organoids derived from
403 BCAM^{lo} cells. Specifically, we show increased expression of *PEG10*, *EPCAM*, and *HMGB3*,
404 indicating that BCAM may confer increased organoid growth by controlling stem cell maintenance or
405 regeneration. In our experimental organoid system, even though BCAM^{lo} organoids form smaller
406 colonies by day 11, assessment of BCAM expression in BCAM^{lo} organoids at endpoint shows that
407 BCAM levels and the frequency of BCAM-expressing cells is comparable to BCAM^{hi} CTBs. This
408 suggests that BCAM expression in progenitor CTBs is dynamic, and that requirements for growth,
409 stemness, or survival result in the induction of BCAM expression. Consistent for a role for BCAM in
410 controlling organoid growth, BCAM silencing also resulted in the formation of smaller organoids,
411 where cell cycle analysis suggests that BCAM regulates progenitor entry/exit into the cell cycle. Future
412 research should focus on how BCAM potentially creates a supportive stem/regenerative cell niche,
413 possibly by mediating specific cell-ECM engagement signals important in progenitor maintenance.
414 The identification of a novel cell surface human CTB progenitor cell marker provides improved
415 methods for isolating and studying the mechanisms regulating human CTB progenitor cells, trophoblast
416 differentiation, and human placental development. We have used single cell RNA sequencing to define
417 trophoblast differentiation trajectories in early human placental development. Importantly, we identify
418 BCAM as a new CTB progenitor marker that confers enhanced clonal growth. Future work is needed to
419 clarify how increased BCAM expression facilitates improved CTB growth, and the exact molecular
420 paths through which this occurs. We hope that future experiments will be able to capitalize on the
421 identification of BCAM as a cell surface CTB progenitor marker through which these cells can be
422 isolated and further studied.
423

424 **MATERIALS AND METHODS**

425 **Patient recruitment and tissue collection**

426 Placental tissues were obtained with approval from the Research Ethics Board on the use of
427 human subjects, University of British Columbia (H13-00640). All samples were collected from women
428 (19 to 39 years of age) providing written informed consent undergoing elective terminations of
429 pregnancy at British Columbia's Women's Hospital, Vancouver, Canada. First trimester placental
430 tissues (*n*=9) were collected from participating women (gestational ages ranging from 5–12 weeks)
431 having confirmed viable pregnancies by ultrasound-measured fetal heartbeat. Patient clinical
432 characteristics i.e. height and weight were additionally obtained to calculate body mass index (BMI:
433 kg/m^2) and all consenting women provided self-reported information via questionnaire to having first
434 hand exposure to cigarette smoke or taken anti-inflammation or anti-hypertensive medications during
435 pregnancy. Patient and sample phenotype metadata are summarized in Supplemental Table 1.

436

437 **Human trophoblast organoids**

438 *Establishment and culture*: Human trophoblast stem cells (hTSC) CT27 (RCB4936), CT29
439 (RCB4937), and CT30 (RCB4938) from Riken BRC Cell Bank, were established from first trimester
440 CTBs by Okae et al (Okae *et al.*, 2018) and used here to generate organoid cultures using a
441 modification of previously described protocols (Haider *et al.*, 2018; Turco *et al.*, 2018). In summary,
442 these cells were re-suspended in ice-cold growth factor-reduced Matrigel (GFR-M, Corning) to a final
443 concentration of 100%. Cell suspensions (40 µl) containing 5-20 x 10^3 cells were carefully seeded in
444 the center of each well of a 24-well plate. Plates were placed at 37°C for 2 minutes. Following this, the
445 plates were turned upside down to promote equal spreading of the cells throughout the Matrigel domes.
446 After 15 minutes, the plates were flipped back to normal and the Matrigel domes were overlaid with
447 0.5 mL pre-warmed trophoblast organoid media containing advanced DMEM/F12 (Gibco), 10 mM
448 HEPES, 1 x B27 (Gibco), 1 x N2 (Gibco), 2 mM L-glutamine (Gibco), 100 µg/ml Primocin
449 (Invivogen), 100 ng/mL R-spondin (PeproTech), 1 µM A83-01 (Tocris), 100 ng/mL rhEGF
450 (PeproTech), 3 µM CHIR99021 (Tocris), and 2 µM Y-27632 (EMD Millipore). Organoids were
451 cultured for 7-21 days.

452 *EVT Differentiation*: EVT differentiation of trophoblast organoids was performed using an
453 adapted of previously published protocols (Okae *et al.*, 2018). In summary, organoids were cultured
454 until > 50% colonies reached at least 100 µm in diameter (~3-5 days). Following this, organoids were
455 maintained in EVT differentiation media containing advanced DMEM/F12, 0.1 mM 2-mercaptoethanol

456 (Gibco), 0.5% penicillin/streptomycin (Gibco), 0.3% BSA (Sigma Aldrich), 1% ITS-X supplement
457 (Gibco), 100 ng/mL NRG1 (Cell Signaling Technology), 7.5 μM A83-01 (Tocris), 4% Knockout
458 Serum Replacement (Gibco). Media exchanged for EVT differentiation media lacking NRG1 around
459 day 7-10 of differentiation following the visible outgrowth of cells. Differentiation was stopped at day
460 7 (D7) for 10X single cell RNA sequencing and flow cytometry analysis. Differentiation was stopped
461 at day 21 (D21) for qPCR analysis.
462
463 **Placental tissue and trophoblast organoid single cell RNA-seq library construction**
464 *Placental tissue:* Healthy placental villi were physically scraped form chorionic membrane by
465 scalpel and enzymatically digested in 0.5 ml collagenase/hyaluronidase and 1.5 ml DMEM/F12 with
466 500 μl penicillin/streptomycin and 500 μl 100X antibiotic/antimycotic at 37˚C for 45 minutes.
467 Placental villi cell suspensions were diluted in 1X Hank's Balanced Salt Solution (HBSS) containing
468 2% FBS, pelleted at 1200 rpm for 5 minutes, and resuspended in 0.25% trypsin-EDTA. The solution
469 was diluted again in 1X HBSS containing 2% FBS, pelleted at 1200 rpm for 5 minutes, and
470 resuspended in dispase and 1 mg/ml DNase I. Liberated cells were enriched by passing digest through
471 through a 40 μm filter.
472 *Trophoblast organoids:* For all organoid cultures, media was aspirated, and organoids were
473 diluted in Cell Recovery Solution at 4˚C for 40 minutes on either culture day 0 in complete media (non-
474 differentiated organoids) or culture day 7 in differentiation media (EVT-differentiated organoids). Cells
475 were then washed with cold PBS and centrifuged at 1000 rpm for 5 minutes. Cells were disaggregated
476 in TrypLE containing 5% DNase I at 37˚C for 7 minutes before the addition of 100 μl complete media.
477 The resulting cell suspension was then sieved through a 40 μm filter.
478 *Library construction*: Single cell suspensions (tissue- and organoid-derived) were stained with
479 7-Aminoactinomycin D (7-AAD) viability marker and live/dead sorted using a Becton Dickinson (BD)
480 FACS Aria. Cell suspensions were loaded onto the 10X Genomics single cell controller for library
481 preparation. Placental villi-derived single cell suspensions were prepared using the chromium single
482 cell 3' reagent v2 chemistry kit, following standard manufacturer protocol for all steps. Non-
483 differentiated and differentiated trophoblast organoid-derived single cell suspensions were prepared
484 using the chromium single cell 3' reagent v3 chemistry kit, following standard manufacturer protocol
485 for all steps. Single cell libraries were sequenced on an Illumina Nextseq 500 instrument at a
486 sequencing depth of 50,000 reads/cell for tissue-derived cells and 150,000 reads/cell for organoid-
487 derived cells. For placental villus samples, the 10X Genomics Cell Ranger version 2.0 software was

488 used for STAR read alignment and counting against the provided GRCh38 reference while the
489 trophoblast organoid samples used the 10X Genomics Cell Ranger version 3.0 software for STAR read
490 alignment and counting against the GRCh38 reference.

491 *Data Repository Integration*: Droplet-based first trimester scRNA-seq decidual and placental
492 tissue data was obtained from the public repository ArrayExpress (available at: E-MTAB-6701)
493 (Vento-Tormo *et al.*, 2018). Raw BAM files were downloaded and pre-processed using 10X Genomics
494 Cell Ranger version 2.0 under identical parameters as previously described for our placental villi and
495 trophoblast organoid samples using the GRCh38 reference. Sample specific metrics are summarized in
496 Supplemental Table 2.

497

498 **Single cell RNA-seq data analysis**

499 *Data pre-processing and quality control*: A total of 50,790 single cells were sequenced and pre-
500 processed using the Seurat R package (Butler *et al.*, 2018; Stuart *et al.*, 2019). To ensure quality cells
501 were used in downstream analyses, cells containing fewer than 1000 detected genes and greater than
502 20% mitochondrial DNA content were removed. Individual samples were scored based on expression
503 of G2/M and S phase cell cycle gene markers, scaled, normalized, and contaminating cell doublets
504 were removed using the DoubletFinder package (McGinnis, Murrow and Gartner, 2019) with default
505 parameters and a doublet formation rate estimated from the number of captured cells. Following pre-
506 processing, all samples were merged and integrated using cell pairwise correspondences between single
507 cells across sequencing batches. During integration, the Pearson residuals obtained from the default
508 regularized negative binomial model were re-computed and scaled to remove latent variation in percent
509 mitochondrial DNA content as well as latent variation resulting from the difference between the G2M
510 and S phase cell cycle scores.

511 *Cell clustering, identification, and trophoblast sub-setting*: Cell clustering was accomplished in
512 Seurat at a resolution of 0.90 using 50 principal components. Cell identity was determined through
513 observation of known gene markers found within the maternal fetal interface (vimentin, CD45, neural
514 cell adhesion molecule, CD14, etc.) and identifying cluster marker genes via the "FindAllMarkers"
515 function using a model-based analysis of single-cell transcriptomics (MAST) GLM-framework
516 implemented in Seurat (Finak *et al.*, 2015). Gene markers were selected as genes with a minimum log
517 fold change value > 0.20 and an adjusted p-value < 0.05 within a specific cluster. Trophoblasts were
518 identified as expressing *KRT7, EGFR, TEAD4, TP63, TFAP2A, TFAP2C, GATA2, GATA3, HLA-G,*
519 *ERVFRD-1* transcripts at a level greater than zero, and *VIM, WARS, PTPRC, DCN, CD34, CD14,*

520 *CD86, CD163, NKG7, KLRD1, HLA-DPA1, HLA-DPB1, HLA-DRA, HLA-DRB1, HLA-DRB5, HLA-*
521 *DQA1* transcripts at a level equal to zero. Trophoblasts were subset and re-clustered in Seurat at a
522 resolution of 0.375 using 30 principal components. As mentioned previously, trophoblast cluster
523 identity was determined through observation of known trophoblast gene marker expression,
524 proliferative gene marker expression, and from unique cluster genes identified by differential
525 expression analysis in Seurat. Trophoblast projections were visualized using Uniform Manifold
526 Approximation and Projections (UMAPs).

527 *Differential gene expression*: Differential expression (DEG) analyses were performed in Seurat
528 using the "FindMarkers" function using a MAST framework on the raw count data. Parameters were
529 limited to genes with a log fold-change difference between groups of 0.20 and genes detected in a
530 minimum 10% cells in each group. Results were filtered for positive gene markers and significant
531 DEGs were taken as having a fold change difference > 0.25 and an adjusted p value < 0.05.

532 *Gene set enrichment analysis*: GSEA analyses were performed in Seurat using the
533 "FindMarkers" function using a MAST framework on the raw count data. Parameters included a
534 minimum log fold-change difference between groups of "–INF", a minimum gene detection of "–INF"
535 in cells in each group, and a minimum difference in the fraction of detected genes within each group of
536 "–INF", allowing all genes to be compared. Results were visualized using the R package
537 EnhancedVolcano (version 1.8.0), with a fold-change cut-off of 0.25 and a p value cut off of 0.00005
538 taken as the thresholds for significance.

539 *Gene ontology*: GO analysis of significant differentially expressed genes was performed using
540 the clusterProfiler R package (Yu *et al.*, 2012) and the top enriched terms (Benjamini-Hochberg
541 corrected p value <0.05) were visualized as dot plots using the R package enrich plot (version 1.10.2).

542 *Pseudotime:* The Monocle2 R package (Trapnell *et al.*, 2014; Qiu, Hill, *et al.*, 2017; Qiu, Mao,
543 *et al.*, 2017) was used to explore the differentiation of progenitor CTBs into specialized SCT and EVT.
544 The trophoblast cell raw counts were loaded into Monocle2 for semi-supervised single cell ordering in
545 pseudotime, taking increased *BCAM* expression to represent cells at the origin and *HLA-G* and
546 *ERVFRD-1* gene expression to indicate progress towards EVT and SCT, respectively. Branched
547 expression analysis modelling (BEAM) was applied to observe the expression of identified trophoblast
548 cluster gene markers and genes related to the WNT, HIPPO, NOTCH, and EGFR signaling pathways
549 over pseudotime, progressing towards either EVT or SCT. Results were visualized using the
550 "plot_cell_trajectory" function. To resolve cytotrophoblast differentiation trajectories at higher
551 resolution, the Monocle3 package (Cao *et al.*, 2019) was utilized. Trophoblast raw counts were input,

552 clustered, and the principal graph was created using the "learn_graph" function. The "order_cells"
553 function was then used to order cells in pseudotime, designating the trophoblast root within the CTB 2
554 state.

555 *Lineage Trajectory*: The Velocyto package (La Manno *et al.*, 2018) was run in terminal using
556 the command line interface to generate sample-specific files containing count matrices of unspliced,
557 spliced, and ambiguous RNA transcript abundances. The velocyto.R implementation of the package
558 was then used to merge each file with its corresponding 10X sample during data pre-processing in
559 Seurat. The final, processed trophoblast object and UMAP embeddings were exported to a Jupyter
560 Notebook and the scVelo Python package (Bergen *et al.*, 2020) was used to read, prepare, and recover
561 holistic trophoblast gene splicing kinetics. Velocities were projected on top of the extracted UMAP
562 embeddings generated in Seurat.

563

564 **Flow cytometry analysis and cell sorting**

565 *Organoid single cell workflow*: Single cells from CT29 organoids were isolated by incubation
566 with Cell Recovery Solution (Corning) for 40 minutes at 4°C. Then, cells were washed in ice-cold PBS
567 and dissociated into single cells using TrypLE^{TM} supplemented with 5% DNAse I for 7 minutes at
568 37°C.

569 *Phenotyping EVT differentiated CT27, CT29, and CT30 organoids*: Following single cell
570 dissociation, organoid cells were stained with EGFR BV605 (clone AY13; 1:50; Biolegend), HLA-G
571 APC (clone MEMG-9; 1:50; Abcam), HLA-ABC Pacific Blue (clone W6/32; 1:100; Biolegend),
572 CD49e/ITGA5 PeCy7 (clone eBioGoH3; 1:200; Thermo Fisher Scientific), CD49f/ITGA6 Alexa 488
573 (clone P1D6; 1:200; Thermo Fisher Scientific), and BCAM BV711 (clone B64; 1:50; BD Biosciences).

574 *Phenotyping BCAM^{hi} and BCAM^{lo} organoids*: Single cells were incubated with anti-human
575 BCAM BV421 (clone B64; 1:50; BD Biosciences), EGFR BV605, and CD49f/ITGA6 PeCy7 for 30
576 minutes in the dark on ice, followed by viability staining with 7-AAD. Samples were analyzed using
577 LSRII (Becton Dickinson) and a minimum of 20,000 events were acquired.

578 *hTSC BCAM$^{hi/lo}$ sorting:* CT29 hTSCs were dissociated using TrypLE^{TM} (Thermo Fisher
579 Scientific) with 5% DNAse I (Sigma Aldrich) for 7 minutes at 37°C. Following resuspension in PBS
580 supplemented with Antibiotic-Antimycotic (Gibco) and 1% P/S (Sigma Aldrich), cells were stained
581 with BCAM BV421 (clone B64; 1:50; BD Biosciences) and EGFR Pecy7 (clone AY13; 1:50;
582 Biolegend) for 30 minutes at 4°C in the dark, followed by incubation with 7-AAD (Thermo Fisher) for
583 viability assessment. CT29 BCAM^{hi} and BCAM^{lo} populations were sorted using a FACS Aria (BD

584 Biosciences).

585 *Cell cycle analysis*: Cell cycle phases were determined on day 3 of organoid culture using
586 7AAD assessment of DNA quantity. A minimum of 5,000 events were collected and cell cycle was
587 analysed using Watson model on FlowJo 10.7.1.

588

589 **Trophoblast organoid growth assay**

590 CT29 sorted BCAM^{hi} and BCAM^{lo} cells were seeded at a density of 5,000 cells in 40 µL of
591 Matrigel in the presence of trophoblast organoid media. Phase contrast images were taken with
592 AxioObserver inverted microscope (Carl Zeiss) using 20X objective, and organoids were further
593 analyzed by qPCR, immunofluorescence, and flow cytometry. Organoid formation efficiency was
594 assessed by measuring organoid number and size (area in µm^2). Images were taken daily and analyzed
595 using imageJ (NIH). The scale was set by measuring the scale bar in pixels (285.5 pixels = 200 µm).

596

597 **RNA isolation**

598 Prior to RNA extraction, organoids were dissociated into single cells as described above. Total
599 RNA was prepared from these cells using RiboZol reagent (VWR Life Science) followed by RNeasy
600 Mini kit (Qiagen) according to manufacturer's protocol. RNA purity was confirmed using a NanoDrop
601 Spectrophotometer (Thermo Fisher Scientific).

602

603 **cDNA synthesis and qPCR**

604 RNA was reverse transcribed using qScript cDNA SuperMix synthesis kit (Quanta Biosciences)
605 and subjected to qPCR (ΔΔCT) analysis, using PowerUP SYBR Green Master Mix (Thermo Fisher
606 Scientific) on a StepOnePlus Real-Time PCR System (Thermo Fisher Scientific) and forward and
607 reverse primer sets for *TEAD4* (F: 5'-CGGCACCATTACCTCCAACG-3'; R: 5'-
608 CTGCGTCATTGTCGATGGGC-3'), *ITGA6* (F: 5'-CACTCGGGAGGACAACGTGA-3'; R: 5'-
609 ACAGCCCTCCCGTTCTGTTG-3'), *CGB* (F: 5'-GCCTCATCCTTGGCGCTAGA-3'; R: 5'-
610 TATACCTCGGGGTTGTGGGG-3'), *CSH1* (F: 5'-GACTGGGCAGATCCTCAAGCA-3'; R: 5'-
611 CCATGCGCAGGAATGTCTCG-3'), *ITGA5* (F: 5'-GGGTCGGGGGCTTCAACTTA-3'; R: 5'-
612 ACACTGACCCCGTCTGTTCC-3'), *HLA-G* (F: 5'-CCCACGCACAGACTGACAGA-3'; R: 5'-
613 AGGTCGCAGCCAATCATCCA-3'), *NOTCH1* (F: 5'-GCCTGAATGGCGGGAAGTGT-3'; R: 5'-
614 TAGTCTGCCACGCCTCTGC-3'), *NOTCH2* (F: 5'-ACTCGGGGCCTACTCTGTGA-3'; R: 5'-
615 TGTCTCCCTCACAACGCTCC-3'), *GAPDH* (F: 5'-AGGGCTGCTTTTAACTCTGGT-3' R: 5'-

616 CCCCACTTGATTTTGGAGGGA-3'). All raw data were analyzed using StepOne Software v2.3
617 (Thermo Fisher Scientific). The threshold cycle values were used to calculate relative gene expression
618 levels. Values were normalized to endogenous *GAPDH* transcripts.
619
620 **Immunofluorescence microscopy**
621 Placental villi (6-12 weeks' gestation; n=2) were fixed in 2% paraformaldehyde overnight at 4
622 °C. Tissues were paraffin embedded and sectioned at 6 μm onto glass slides. Immunofluorescence was
623 performed as previously described. Briefly, organoids or placental tissues underwent antigen retrieval
624 by heating slides in a microwave for 5 X 2-minute intervals in citrate buffer (pH 6.0). Sections were
625 incubated with sodium borohydride for 5 minutes at room temperature (RT), followed by Triton X-100
626 permeabilization for (Aghababaei *et al.*, 2015) 5 minutes, RT. Slides were blocked in 5% normal goat
627 serum/0.1% saponin for 1hr, RT, and incubated with combinations of the indicated antibodies
628 overnight at 4 °C: mouse monoclonal anti-HLA-G (clone 4H84; 1:100; Exbio, Vestec, Czech
629 Republic); rabbit monoclonal anti-cytokeratin 7 (clone SP52; 1:50; Ventana Medical Systems), rabbit
630 polyclonal anti-BCAM (1:100; Abcam); mouse monoclonal anti-hCG beta (clone 5H4-E2; 1:100;
631 Abcam), anti-BrdU (1:1000, Bu20a, Cell Signaling Technology). Following overnight incubation,
632 sections and coverslips were washed with PBS and incubated with Alexa Fluor goat anti-rabbit 568 and
633 goat anti-mouse 488 conjugated secondary antibodies (Life Technologies, Carlsbad, CA) for 1h at RT,
634 washed in PBS and mounted using ProLong Gold mounting media containing DAPI (Life
635 Technologies).
636 Slides were imaged with an AxioObserver inverted microscope (Car Zeiss, Jena, Germany)
637 using 20X Plan-Apochromat/0.80NA or 40X Plan-Apochromat oil/1.4NA objectives (Carl Zeiss). An
638 ApoTome .2 structured illumination device (Carl Zeiss) set at full Z-stack mode and 5 phase images
639 was used for image acquisition.
640
641 **siRNA knockdown of *BCAM***
642 Two BCAM-targeting siRNAs (siBCAM #1, siBCAM #2; Dharmacon) were transfected into
643 CT29 hTSCs using Lipofectamine RNAiMAX (Thermo Fisher) at a concentration of 100 nM. For
644 controls, cells were transfected with ON-TARGETplus non-silencing siRNA (siCTRL; Cat# D-
645 001810-01-20; Dharmacon) or cultured in the presence of transfection reagent alone (non-treated; NT).
646 CT29 hTSCs cultured in 2D were initially forward-transfected using Lipofectamine RNAiMAX
647 (Thermo Fisher) to achieve efficient *BCAM* silencing prior to organoid establishment. Following 48 h,

hTSCs cells were transfected with BCAM and CTRL siRNAs for a second time following a reverse transfection approach and embedded in Matrigel to initiate 3D trophoblast organoids. Following 3- or 7-days post-transfection, organoids were either cell dissociated from Matrigel using Cell Recovery Solution (BD Biosciences) for BCAM cell surface quantification using flow cytometry, or fixed in 4% paraformaldehyde, embedded in paraffin, and sectioned onto glass slides for IF assessment of BCAM, respectively.

BrdU incorporation assay

Pulse-chase labeling with BrdU (Sigma-Aldrich) was conducted on CT29 hTSC-derived organoids. Two days following 3D hTSC organoid establishment and reverse control (siCTLR) and BCAM siRNA (siBCAM#1, siBCAM#2) transfection, organoids were exposed to a 4-hr pulse with culture media containing 10 μM of BrdU. Following 4 hr of labelling, organoids were washed in PBS and fixed in 4% PFA overnight. Organoids were paraffin embedded and sectioned for immunofluorescence microscopy. Immunofluorescent staining with anti-BrdU antibody (1:200, Bu20a, Sigma-Aldrich) with the addition of a 30-minute incubation in 2M hydrochloric acid between permeabilization and sodium borohydride steps.

Statistical analysis

Data are reported as median values with standard deviations. All calculations were carried out using GraphPad Prism 9 software (San Diego, CA). For single comparisons, Mann-Whitney non-parametric unpaired t-tests were performed. For multiple comparisons, one-way Kruskal-Wallis ANOVA followed by Dunn's multiple comparison test was performed. One-way ANOVA followed by Tukey post-test were performed for all other multiple comparisons. The differences were accepted as significant at $P < 0.05$. For scRNA-seq statistical analyses, please refer to scRNA-seq analysis sections in methods.

DATA AVAILABILITY/ACCESSION NUMBER

The ArrayExpress accession number for the publicly available data reported in this paper is: E-MTAB-6701

AUTHOR CONTRIBUTIONS

AGB designed the research. AGB, MS, JB, BC, JW, SY, JT, HTL, PML performed experiments and analysed data. AGB, MS, JB, and BC wrote the paper. All authors read and approved the manuscript.

FUNDING

This work was supported by a Natural Sciences and Engineering Research Council of Canada (NSERC; RGPIN-2014-04466) Discovery Grant and Canadian Institutes of Health Research 201809PJT-407571-CIA-CAAA) operating grants (to AGB), a British Columbia Children's Hospital Catalyst Grant (to PML), and a Canadian Institutes of Health Research Master's graduate studentship (to MS).

ACKNOWLEDGEMENTS

The authors extend their sincere gratitude to the hard work of staff at British Columbia's Women's Hospital's CARE Program for recruiting participants to our study and the staff at the University of British Columbia Biomedical Research Centre, especially Yiwei Zhao and Ryan Vander Werff, for assistance with all drop-seq library preparation and sequencing.

COMPETING INTERESTS

The authors declare that no competing interests exist.

699 **REFERENCES**

700 Aghababaei, M. *et al.* (2015) 'ADAM12-directed ectodomain shedding of E-cadherin potentiates
701 trophoblast fusion', *Cell Death & Differentiation*, 22(12), pp. 1970–1984. doi:
702 10.1038/cdd.2015.44.

703 Bergen, V. *et al.* (2020) 'Generalizing RNA velocity to transient cell states through dynamical
704 modeling', *Nature Biotechnology*, 38(12), pp. 1408–1414. doi: 10.1038/s41587-020-0591-3.

705 Burton, G. J., Cindrova-Davies, T. and Turco, M. Y. (2020) 'Review: Histotrophic nutrition and the
706 placental-endometrial dialogue during human early pregnancy', *Placenta*, 102, pp. 21–26. doi:
707 10.1016/j.placenta.2020.02.008.

708 Butler, A. *et al.* (2018) 'Integrating single-cell transcriptomic data across different conditions,
709 technologies, and species', *Nature Biotechnology*, 36(5), pp. 411–420. doi: 10.1038/nbt.4096.

710 Cao, J. *et al.* (2019) 'The single-cell transcriptional landscape of mammalian organogenesis',
711 *Nature*, 566(7745), pp. 496–502. doi: 10.1038/s41586-019-0969-x.

712 Capurro, M. *et al.* (2014) 'Glypican-3 binds to Frizzled and plays a direct role in the stimulation of
713 canonical Wnt signaling', *Journal of Cell Science*, 127(7), pp. 1565–1575. doi: 10.1242/jcs.140871.

714 Chang, C.-W., Wakeland, A. K. and Parast, M. M. (2018) 'Trophoblast lineage specification,
715 differentiation and their regulation by oxygen tension', *Journal of Endocrinology*, 236(1), pp. R43–
716 R56. doi: 10.1530/JOE-17-0402.

717 Finak, G. *et al.* (2015) 'MAST: a flexible statistical framework for assessing transcriptional
718 changes and characterizing heterogeneity in single-cell RNA sequencing data', *Genome Biology*,
719 16(1), p. 278. doi: 10.1186/s13059-015-0844-5.

720 Fowden, A. L. *et al.* (2015) 'Review: Endocrine regulation of placental phenotype', *Placenta*, 36,
721 pp. S50–S59. doi: 10.1016/j.placenta.2014.11.018.

722 Guadall, A. *et al.* (2019) 'Dimerization and phosphorylation of Lutheran/basal cell adhesion
723 molecule are critical for its function in cell migration on laminin', *Journal of Biological Chemistry*,
724 294(41), pp. 14911–14921. doi: 10.1074/jbc.RA119.007521.

725 Haider, S. *et al.* (2014) 'Notch Signaling Plays a Critical Role in Motility and Differentiation of
726 Human First-Trimester Cytotrophoblasts', *Endocrinology*, 155(1), pp. 263–274. doi:
727 10.1210/en.2013-1455.

728 Haider, S. *et al.* (2016) 'Notch1 controls development of the extravillous trophoblast lineage in
729 the human placenta', *Proceedings of the National Academy of Sciences*, 113(48), pp. E7710–E7719.
730 doi: 10.1073/pnas.1612335113.

731 Haider, S. *et al.* (2018) 'Self-Renewing Trophoblast Organoids Recapitulate the Developmental
732 Program of the Early Human Placenta', *Stem Cell Reports*, 11(2), pp. 537–551. doi:
733 10.1016/j.stemcr.2018.07.004.

734 Jauniaux, E., Moffett, A. and Burton, G. J. (2020) 'Placental Implantation Disorders', *Obstetrics and*

735 *Gynecology Clinics of North America*, 47(1), pp. 117–132. doi: 10.1016/j.ogc.2019.10.002.

736 Jiang, Y., He, X. and Howe, P. H. (2012) 'Disabled-2 (Dab2) inhibits Wnt/β-catenin signalling by
737 binding LRP6 and promoting its internalization through clathrin: Dab2 regulates clathrin-
738 mediated endocytosis of LRP6', *The EMBO Journal*, 31(10), pp. 2336–2349. doi:
739 10.1038/emboj.2012.83.

740 Kannan, K. *et al.* (2015) 'Recurrent *BCAM-AKT2* fusion gene leads to a constitutively activated
741 AKT2 fusion kinase in high-grade serous ovarian carcinoma', *Proceedings of the National*
742 *Academy of Sciences*, 112(11), pp. E1272–E1277. doi: 10.1073/pnas.1501735112.

743 Kikkawa, Y. *et al.* (2013) 'The Lutheran/Basal Cell Adhesion Molecule Promotes Tumor Cell
744 Migration by Modulating Integrin-mediated Cell Attachment to Laminin-511 Protein*', *Journal of*
745 *Biological Chemistry*, 288(43), pp. 30990–31001. doi: 10.1074/jbc.M113.486456.

746 Knöfler, M. *et al.* (2019) 'Human placenta and trophoblast development: key molecular
747 mechanisms and model systems', *Cellular and Molecular Life Sciences*, 76(18), pp. 3479–3496.
748 doi: 10.1007/s00018-019-03104-6.

749 La Manno, G. *et al.* (2018) 'RNA velocity of single cells', *Nature*, 560(7719), pp. 494–498. doi:
750 10.1038/s41586-018-0414-6.

751 Lee, C. Q. E. *et al.* (2016) 'What Is Trophoblast? A Combination of Criteria Define Human First-
752 Trimester Trophoblast', *Stem Cell Reports*, 6(2), pp. 257–272. doi: 10.1016/j.stemcr.2016.01.006.

753 Lee, C. Q. E. *et al.* (2018) 'Integrin α2 marks a niche of trophoblast progenitor cells in first
754 trimester human placenta', *Development*, 145(16), p. dev162305. doi: 10.1242/dev.162305.

755 Liu, Y. *et al.* (2018) 'Single-cell RNA-seq reveals the diversity of trophoblast subtypes and
756 patterns of differentiation in the human placenta', *Cell Research*, 28(8), pp. 819–832. doi:
757 10.1038/s41422-018-0066-y.

758 McGinnis, C. S., Murrow, L. M. and Gartner, Z. J. (2019) 'DoubletFinder: Doublet Detection in
759 Single-Cell RNA Sequencing Data Using Artificial Nearest Neighbors', *Cell Systems*, 8(4), pp. 329-
760 337.e4. doi: 10.1016/j.cels.2019.03.003.

761 Moffett, A., Chazara, O. and Colucci, F. (2017) 'Maternal allo-recognition of the fetus', *Fertility and*
762 *Sterility*, 107(6), pp. 1269–1272. doi: 10.1016/j.fertnstert.2017.05.001.

763 Nemeth, M. J., Kirby, M. R. and Bodine, D. M. (2006) 'Hmgb3 regulates the balance between
764 hematopoietic stem cell self-renewal and differentiation', *Proceedings of the National Academy of*
765 *Sciences*, 103(37), pp. 13783–13788. doi: 10.1073/pnas.0604006103.

766 Okae, H. *et al.* (2018) 'Derivation of Human Trophoblast Stem Cells', *Cell Stem Cell*, 22(1), pp. 50-
767 63.e6. doi: 10.1016/j.stem.2017.11.004.

768 Papuchova, H. *et al.* (2020) 'Three types of HLA-G+ extravillous trophoblasts that have distinct
769 immune regulatory properties', *Proceedings of the National Academy of Sciences*, 117(27), pp.
770 15772–15777. doi: 10.1073/pnas.2000484117.

771 Pollheimer, J. *et al.* (2018) 'Regulation of Placental Extravillous Trophoblasts by the Maternal
772 Uterine Environment', *Frontiers in Immunology*, 9, p. 2597. doi: 10.3389/fimmu.2018.02597.

773 Qiu, X., Mao, Q., *et al.* (2017) 'Reversed graph embedding resolves complex single-cell
774 trajectories', *Nature Methods*, 14(10), pp. 979–982. doi: 10.1038/nmeth.4402.

775 Qiu, X., Hill, A., *et al.* (2017) 'Single-cell mRNA quantification and differential analysis with
776 Census', *Nature Methods*, 14(3), pp. 309–315. doi: 10.1038/nmeth.4150.

777 Saha, B. *et al.* (2020) 'TEAD4 ensures postimplantation development by promoting trophoblast
778 self-renewal: An implication in early human pregnancy loss', *Proceedings of the National Academy*
779 *of Sciences*, 117(30), pp. 17864–17875. doi: 10.1073/pnas.2002449117.

780 Stuart, T. *et al.* (2019) 'Comprehensive Integration of Single-Cell Data', *Cell*, 177(7), pp. 1888-
781 1902.e21. doi: 10.1016/j.cell.2019.05.031.

782 Suryawanshi, H. *et al.* (2018) 'A single-cell survey of the human first-trimester placenta and
783 decidua', *Science Advances*, 4(10), p. eaau4788. doi: 10.1126/sciadv.aau4788.

784 Tilburgs, T. *et al.* (2015) 'Human HLA-G+ extravillous trophoblasts: Immune-activating cells that
785 interact with decidual leukocytes', *Proceedings of the National Academy of Sciences*, 112(23), pp.
786 7219–7224. doi: 10.1073/pnas.1507977112.

787 Trapnell, C. *et al.* (2014) 'The dynamics and regulators of cell fate decisions are revealed by
788 pseudotemporal ordering of single cells', *Nature Biotechnology*, 32(4), pp. 381–386. doi:
789 10.1038/nbt.2859.

790 Treissman, J. *et al.* (2020) 'Low oxygen enhances trophoblast column growth by potentiating
791 differentiation of the extravillous lineage and promoting LOX activity', *Development*, 147(2), p.
792 dev181263. doi: 10.1242/dev.181263.

793 Turco, M. Y. *et al.* (2018) 'Trophoblast organoids as a model for maternal–fetal interactions
794 during human placentation', *Nature*, 564(7735), pp. 263–267. doi: 10.1038/s41586-018-0753-3.

795 Turco, M. Y. and Moffett, A. (2019) 'Development of the human placenta', *Development*, 146(22),
796 p. dev163428. doi: 10.1242/dev.163428.

797 Vento-Tormo, R. *et al.* (2018) 'Single-cell reconstruction of the early maternal–fetal interface in
798 humans', *Nature*, 563(7731), pp. 347–353. doi: 10.1038/s41586-018-0698-6.

799 Walentin, K. *et al.* (2015) 'A Grhl2-dependent gene network controls trophoblast branching
800 morphogenesis', *Development (Cambridge, England)*, 142(6), pp. 1125–1136. doi:
801 10.1242/dev.113829.

802 Wang, S. *et al.* (2015) 'DACT2 is a functional tumor suppressor through inhibiting Wnt/β-catenin
803 pathway and associated with poor survival in colon cancer', *Oncogene*, 34(20), pp. 2575–2585.
804 doi: 10.1038/onc.2014.201.

805 Yu, G. *et al.* (2012) 'clusterProfiler: an R Package for Comparing Biological Themes Among Gene

806 Clusters', *OMICS: A Journal of Integrative Biology*, 16(5), pp. 284–287. doi:
807 10.1089/omi.2011.0118.

808 Zen, Q. *et al.* (1999) 'Critical Factors in Basal Cell Adhesion Molecule/Lutheran-mediated
809 Adhesion to Laminin', *Journal of Biological Chemistry*, 274(2), pp. 728–734. doi:
810 10.1074/jbc.274.2.728.

811 Zhou, Y. *et al.* (1997) 'Human cytotrophoblasts adopt a vascular phenotype as they differentiate.
812 A strategy for successful endovascular invasion?', *Journal of Clinical Investigation*, 99(9), pp.
813 2139–2151. doi: 10.1172/JCI119387.

814

815

816 **TITLES AND LEGENDS TO FIGURES**

817 **Figure 1: Single cell characterization of first trimester trophoblasts**

818 **(A)** Schematic of a first trimester chorionic villous including anatomical representations of both an
819 anchoring villous and floating villous. Highlighted are trophoblast sub-populations and the villous and
820 extravillous cell differentiation trajectories: cytotrophoblast (CTB), column cytotrophoblast (cCTB),
821 syncytiotrophoblast (SCT), and invasive extravillous trophoblast (EVT). **(B)** Uniform Manifold
822 Approximation and Projection (UMAP) plot of 7798 captured trophoblasts, demonstrating 8 distinct
823 trophoblast clusters: CTB1-4, cCTB1-2, SCTp, and EVT. **(C)** Heatmap showing the average expression
824 of known trophoblast and proliferation gene markers in each trophoblast cluster. Cell cluster names and
825 colours correspond to those in Figure 1C. **(D)** Proportion of early first trimester trophoblasts in each
826 scRNA-seq-defined state in early (6-7 weeks) and late (9-12 weeks) gestational time-points.

Figure 1

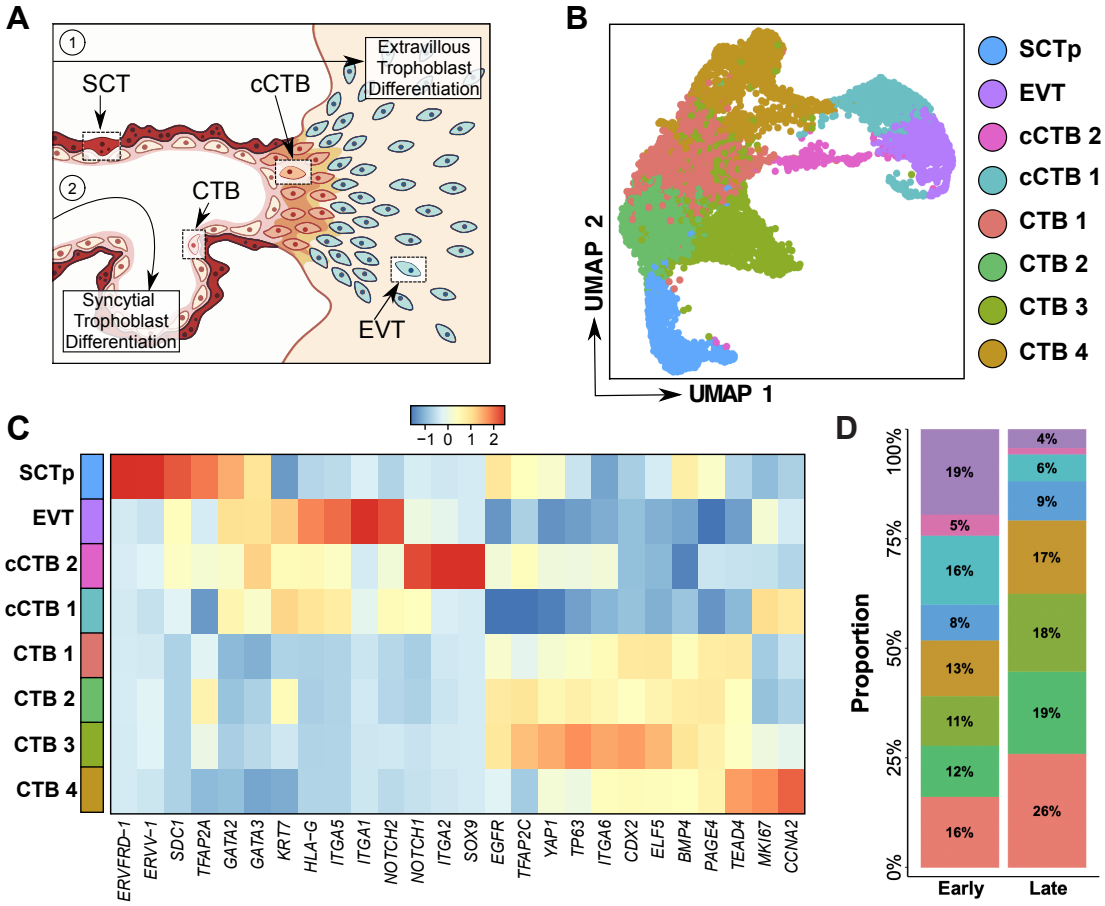
A
1
SCT
cCTB
Extravillous Trophoblast Differentiation
2
CTB
Syncytial Trophoblast Differentiation
EVT
B
UMAP 2
UMAP 1
SCTp
EVT
cCTB 2
cCTB 1
CTB 1
CTB 2
CTB 3
CTB 4
C
−1 0 1 2
SCTp
EVT
cCTB 2
cCTB 1
CTB 1
CTB 2
CTB 3
CTB 4
ERVFRD-1
ERVV-1
SDC1
TFAP2A
GATA2
GATA3
KRT7
HLA-G
ITGA5
ITGA1
NOTCH2
NOTCH1
ITGA2
SOX9
EGFR
TFAP2C
YAP1
TP63
ITGA6
CDX2
ELF5
BMP4
PAGE4
TEAD4
MKI67
CCNA2
D
Proportion
0%
25%
50%
75%
100%
19%
5%
16%
8%
13%
11%
12%
16%
4%
6%
9%
17%
18%
19%
26%
Early
Late

827 **Figure 2: scVelo-informed cell differentiation identifies a primitive CTB origin.**
828 **(A)** UMAP plot overlain with projected RNA velocity (scVelo) vector field, indicating trophoblast
829 directionality (represented by the velocity arrows) away from a putative origin towards endpoint SCTp
830 and EVT states. Cell cluster names and colors correspond to those in Figure 1C. **(B)** UMAP plots
831 showing gene expression (red) of progenitor- and stem cell-associated genes in all scRNA-seq-
832 informed trophoblast states. **(C)** Venn diagram comparing elevated genes within CTB states 2 and 3.
833 Highlighted are genes related to WNT and EGFR signaling pathways, genes involved in extracellular
834 matrix (ECM) interactions, and miscellaneous (Misc) genes of interest. **(D)** A heatmap was constructed
835 using inferred pseudotime and the top 23 up-regulated genes in CTB2. Included within the heatmap are
836 known genes that align with the CTB (CDX2, TEAD4, EPCAM, TP63, YAP1, ELF5), the SCT
837 (ERVFRD-1) and EVT (HLA-G) states. **(E)** scVelo-overlaid UMAP and violin plots showing *BCAM*
838 levels in all first trimester trophoblast states.

Figure 2

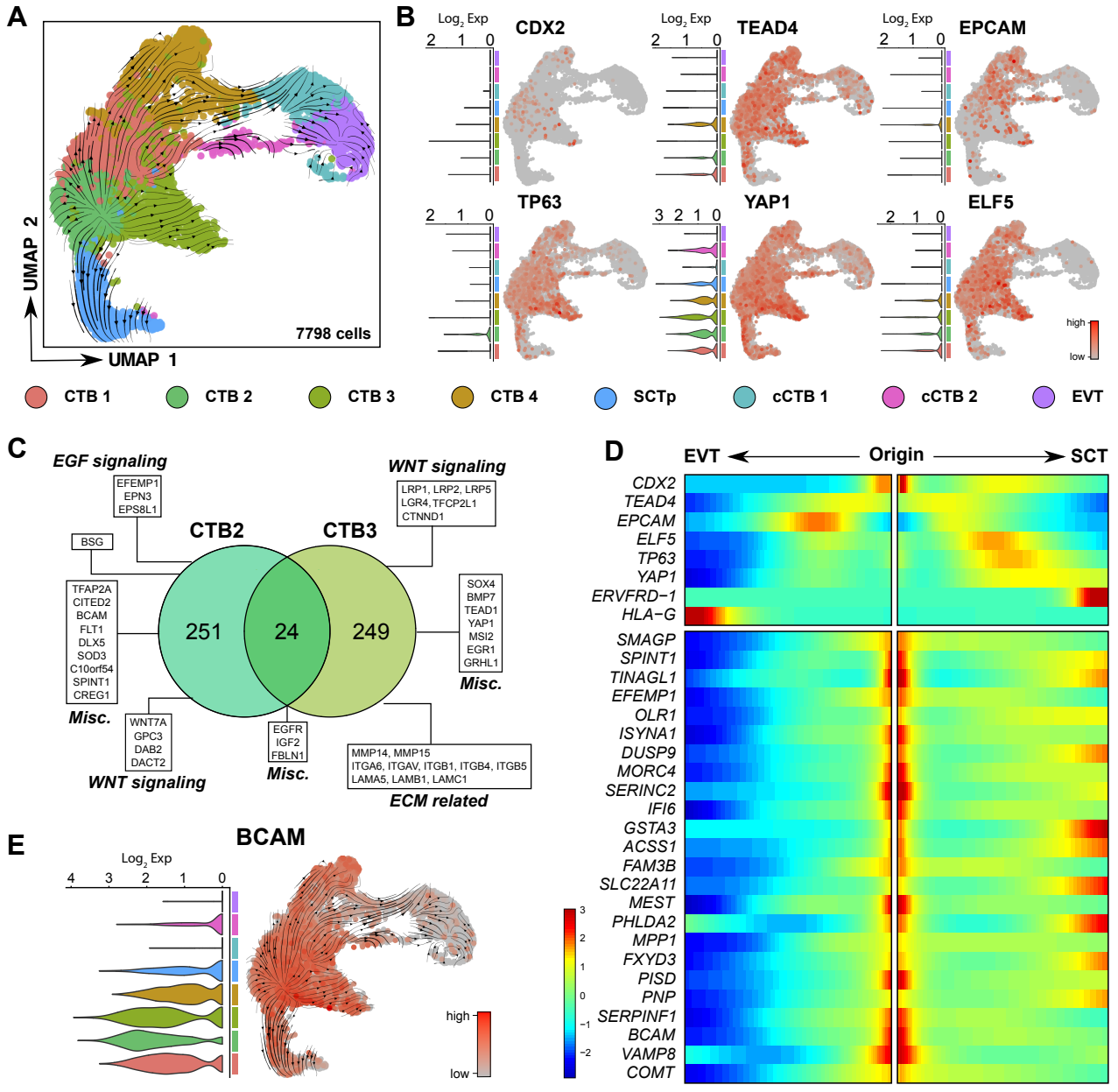
A
UMAP 2
UMAP 1
7798 cells
B
Log2 Exp
CDX2
TEAD4
EPCAM
TP63
YAP1
ELF5
high
low
CTB 1
CTB 2
CTB 3
CTB 4
SCTp
cCTB 1
cCTB 2
EVT
C
EGF signaling
EFEMP1
EPN3
EPS8L1
BSG
WNT signaling
LRP1, LRP2, LRP5
LGR4, TFCP2L1
CTNND1
CTB2
CTB3
251
24
249
TFAP2A
CITED2
BCAM
FLT1
DLX5
SOD3
C10orf54
SPINT1
CREG1
Misc.
SOX4
BMP7
TEAD1
YAP1
MSI2
EGR1
GRHL1
Misc.
WNT7A
GPC3
DAB2
DACT2
WNT signaling
EGFR
IGF2
FBLN1
Misc.
MMP14, MMP15
ITGA6, ITGAV, ITGB1, ITGB4, ITGB5
LAMA5, LAMB1, LAMC1
ECM related
D
EVT
Origin
SCT
CDX2
TEAD4
EPCAM
ELF5
TP63
YAP1
ERVFRD−1
HLA−G
SMAGP
SPINT1
TINAGL1
EFEMP1
OLR1
ISYNA1
DUSP9
MORC4
SERINC2
IFI6
GSTA3
ACSS1
FAM3B
SLC22A11
MEST
PHLDA2
MPP1
FXYD3
PISD
PNP
SERPINF1
BCAM
VAMP8
COMT
E
BCAM
Log2 Exp
high
low

839 **Figure 3: scRNA-seq analyses in hTSC organoids recapitulates a primitive CTB origin**
840 **(A)** Bright field microscopy images of regenerative (Wnt+) and EVT-differentiated (Wnt-) hTSC-
841 derived organoids following 10 days of culture. Bar = 400 μm. **(B)** Relative measurement of mRNA
842 levels by qPCR in EVT-differentiated hTSC-derived organoids (CT27, CT29, CT30) over 21 days (D)
843 of culture. Shown are CTB/progenitor (*TEAD4, ITGA6*), syncytial (*CGB, CSH1*), immature EVT
844 (*ITGA5, NOTCH1*), and mature EVT (*NOTCH2, HLA-G*) genes. Each hTSC line was differentiated as
845 one (n=1) replicate. **(C)** Representative flow cytometry plots showing cell frequencies of HLA-G,
846 CD49e, and HLA-ABC positive cells in regenerative (Wnt+) and EVT-differentiated hTSC-derived
847 (CT27) organoids. CT27 differentiation was performed on three (n=3) independent times. **(D)** UMAP
848 and gene heatmap plots of combined CT27, CT29, and CT30 single cell hTSCs following culture in
849 regenerative (Wnt+) and EVT-differentiated (Wnt-) conditions after 7 days in culture. UMAP plots are
850 overlain with projected RNA velocity (scVelo) vector field, demonstrating 7 distinct trophoblast
851 clusters representing 3 states (CTB1, CTB2, CTB3, bipotent cCTB, EVT1, EVT2, SCTp). Heatmap
852 shows the average expression of trophoblast- and proliferation-associated genes in each cell state. **(E)**
853 UMAP and gene heatmap plots derived from individual hTSC lines (CT27, 2259 cells; CT29, 1446
854 cells; CT30, 2604 cells) subjected to scRNA-seq analyses. UMAP plots are overlain with projected
855 RNA velocity vector field, demonstrating 5 distinct trophoblast clusters in each hTSC line. **(F)** Venn
856 diagram comparing genes shared and distinct between CTB2 in chorionic villi and CTB1 in hTSC
857 organoids. **(G)** Volcano plot showing differentially expressed genes between CTB2 in chorionic villi
858 and CTB1 in organoids. **(H)** Top pathways enriched in CTB2 (villi) and CTB1 (organoid) gene
859 signatures. UMAP plots showing expression of BCAM (red) and velocity arrows in **(I)** combined
860 (CT27, CT29, CT30) and **(J)** segregated hTSC-derived organoid cells/states.

Figure 3

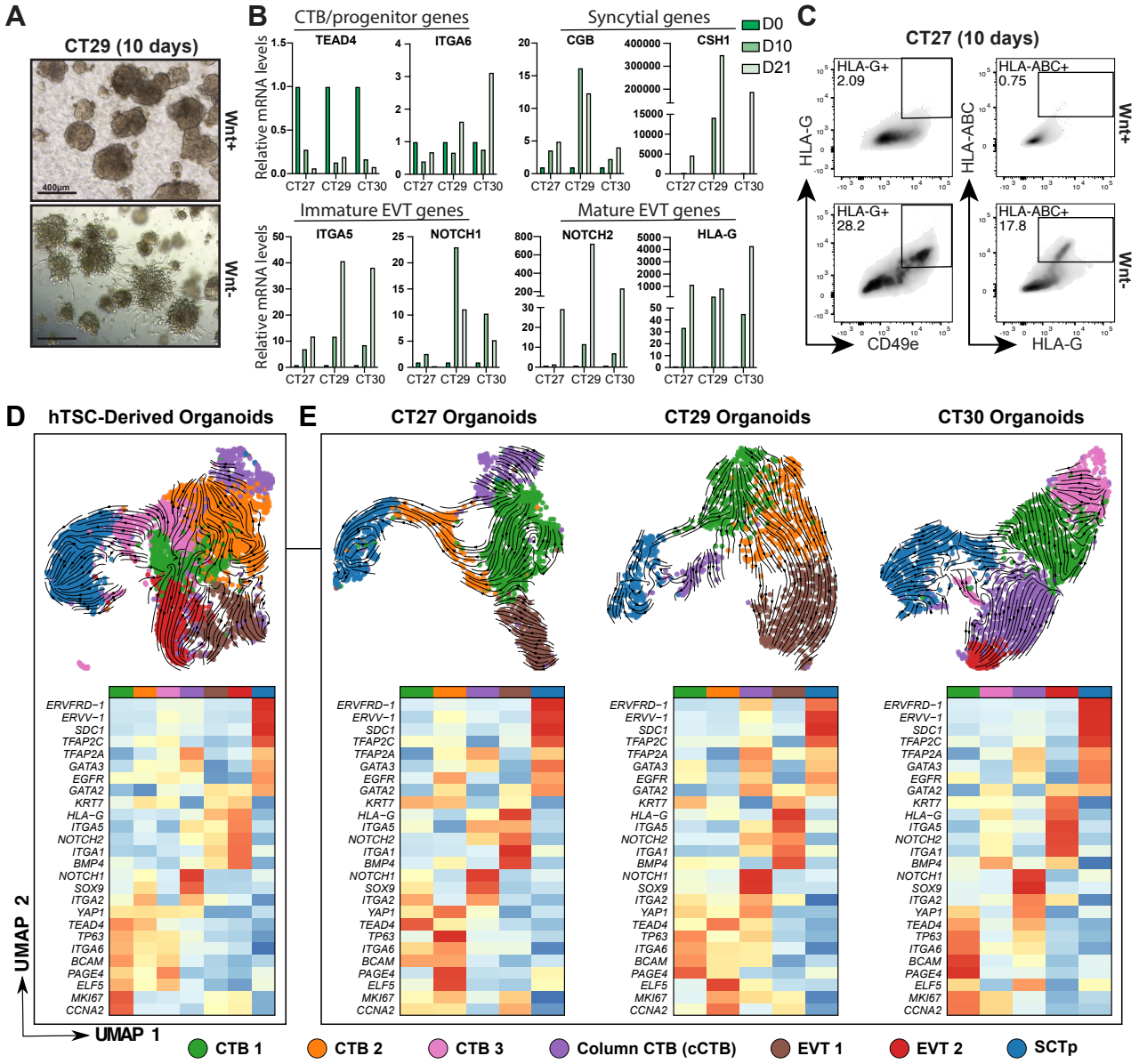
A
CT29 (10 days)
Wnt+
Wnt-
400µm
B
CTB/progenitor genes
Syncytial genes
D0
D10
D21
TEAD4
ITGA6
CGB
CSH1
Relative mRNA levels
Immature EVT genes
Mature EVT genes
ITGA5
NOTCH1
NOTCH2
HLA-G
CT27
CT29
CT30
C
CT27 (10 days)
HLA-G+
2.09
HLA-ABC+
0.75
HLA-G+
28.2
HLA-ABC+
17.8
HLA-G
HLA-ABC
CD49e
Wnt+
Wnt-
D
hTSC-Derived Organoids
E
CT27 Organoids
CT29 Organoids
CT30 Organoids
ERVFRD-1
ERVV-1
SDC1
TFAP2C
TFAP2A
GATA3
EGFR
GATA2
KRT7
HLA-G
ITGA5
NOTCH2
ITGA1
BMP4
NOTCH1
SOX9
ITGA2
YAP1
TEAD4
TP63
ITGA6
BCAM
PAGE4
ELF5
MKI67
CCNA2
UMAP 2
UMAP 1
CTB 1
CTB 2
CTB 3
Column CTB (cCTB)
EVT 1
EVT 2
SCTp
F
CTB2
Placental villi
1430
481
1406
CTB1
Organoid
G
IFI27
NEAT1
CCNE1
LGALS1
DUSP9
PAGE4
FOXO4
PHLDA2
−Log10P
CTB1
Organoid
CTB2
Placental villi
Log2 fold change
H
Trophoblast organoid (CTB1)
Placental villi (CTB2)
cell division
microtubule cytoskeleton organization
microtubule-based process
polymeric cytoskeletal fiber
respiratory chain complex
mitochondrial respirasome
respirasome
inorganic molecular entity transmembrane transporter activity
GeneRatio
I
BCAM (CT27, CT29, CT30)
J
BCAM (CT27)
BCAM (CT29)
BCAM (CT30)

861 **Figure 4: BCAM enrichment establishes a growth advantage in trophoblast organoids**
862 **(A)** Immunofluorescence (IF) images of BCAM and keratin-7 (KRT7), human chorionic gonadotrophin
863 (hCG), and HLA-G in early (6.3 weeks) and late (11.2 weeks) first trimester placental villi. Nuclei are
864 stained with DAPI (white). Bars = 100μm. **(B)** IF images of BCAM, hCG and Ki67 in hTSC-derived
865 organoid (CT29) cultured in regenerative (Wnt+) media for 7 days. **(C)** Cell sorting workflow for
866 isolating $BCAM^{hi}$ and $BCAM^{lo}$ EGFR+ CTBs in hTSC (CT29)-derived organoids. **(D)** Bright field
867 images of hTSC (CT29) $BCAM^{hi}$ and $BCAM^{lo}$ –derived organoids cultured over 11 days in
868 regenerative Wnt+ media. Bars = 200μm. **(E)** Colony area (μm^2) of $BCAM^{hi}$ and $BCAM^{lo}$ hTSC
869 (CT29)-derived organoids cultured over 11 days (D). Each condition was performed on three (n=3)
870 independent occasions. Median values are shown and statistical analyses were performed using a 2way
871 ANOVA, multiple comparisons were controlled for using a Bonferroni post-test; significance $p < 0.05$.
872 ** = $p < 0.01$; **** = $p < 0.0001$. **(F)** Flow cytometric panels showing expression of BCAM and EGFR
873 in $BCAM^{hi}$ and $BCAM^{lo}$, CT29-derived organoids following 11 days of culture. **(G)** Heatmap showing
874 levels of select differentially expressed genes from CTB expressing high (hi) or low (lo) levels of
875 *BCAM* in the scRNA-seq defined CTB1 state of CT29-derived organoids following 7 days of culture.

Figure 4

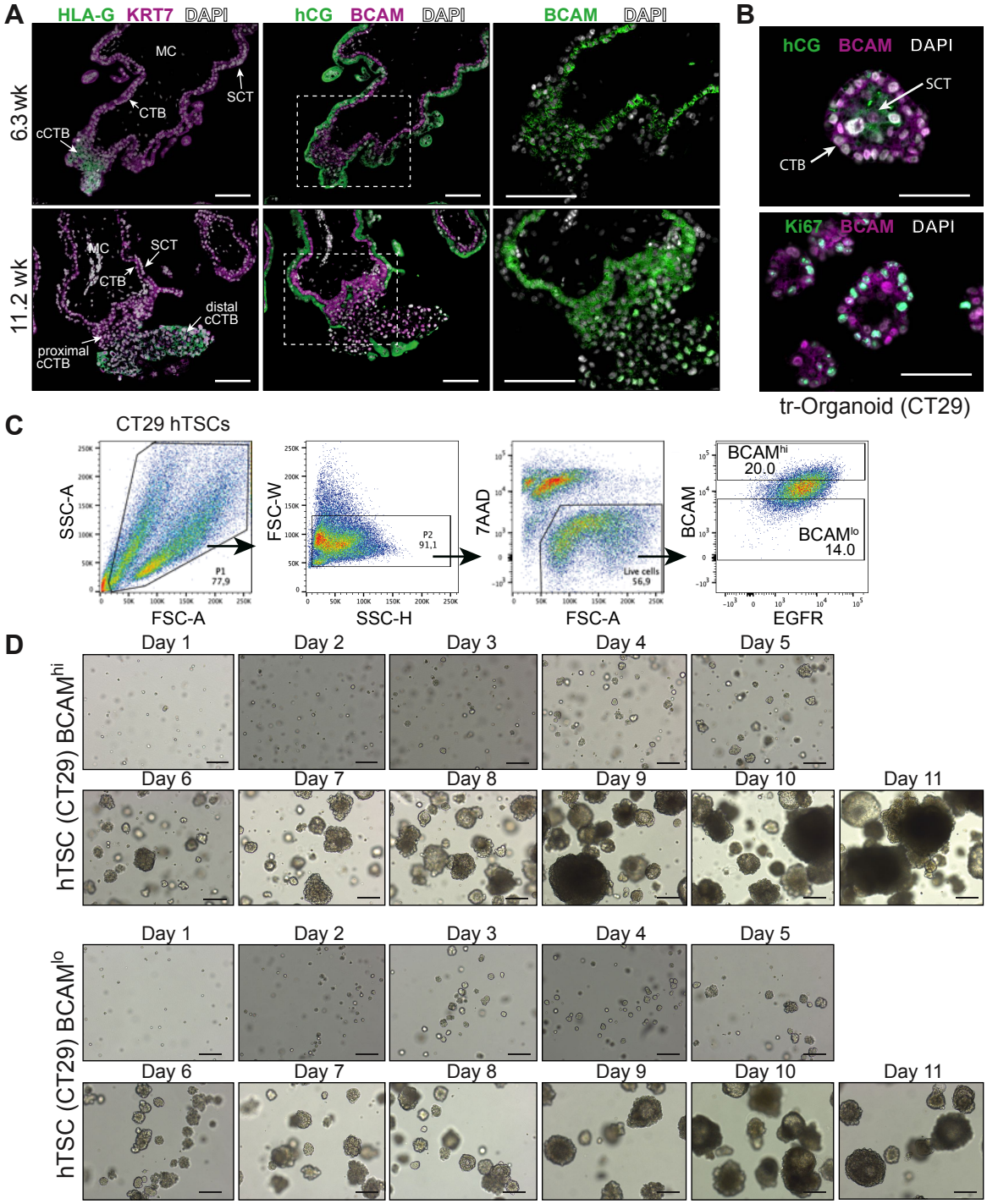
A
HLA-G KRT7 DAPI
hCG BCAM DAPI
BCAM DAPI
6.3 wk
11.2 wk
MC
SCT
CTB
cCTB
distal cCTB
proximal cCTB
B
hCG BCAM DAPI
SCT
CTB
Ki67 BCAM DAPI
tr-Organoid (CT29)
C
CT29 hTSCs
SSC-A
FSC-A
P1 77,9
FSC-W
SSC-H
P2 91,1
7AAD
FSC-A
Live cells 56,9
BCAM
EGFR
BCAM^hi 20.0
BCAM^lo 14.0
D
hTSC (CT29) BCAM^hi
hTSC (CT29) BCAM^lo
Day 1
Day 2
Day 3
Day 4
Day 5
Day 6
Day 7
Day 8
Day 9
Day 10
Day 11
E
BCAM^lo
BCAM^hi
Area (µm²)
80000
60000
40000
20000
0
D1 D2 D3 D4 D5 D6 D7 D8 D9 D10 D11
****
***
**
F
CT29 BCAM^hi
BCAM^hi 91.3
BCAM^lo 6.1
CT29 BCAM^lo
BCAM^hi 69.9
BCAM^lo 20.8
BCAM
EGFR
G
BCAM
Lo Hi
BCAM
LRPAP1
PEG10
SPINT2
EPCAM
LAMB1
PDLIM1
HMGB3
CTB 1

876 **Figure 5: BCAM promotes CTB organoid growth**

877 **(A)** IF images of BCAM in CT29 organoids transfected with control siRNA (ciCTRL) and BCAM-
878 targeting siRNAs (siBCAM#1, siBCAM#2). Nuclei are stained with DAPI. Bars = 100 μm. **(B)**
879 Representative flow cytometry plots showing BCAM levels in control (NT, siCTRL) and BCAM-
880 silenced (siBCAM#1, siBCAM#2) CT29 organoids. FMO = fluorescence minus one. Bar graph to the
881 right shows quantification of BCAM median fluorescence intensity (MFI). Statistical analyses between
882 groups were performed using ANOVA and two-tailed Tukey post-test; significance $p < 0.05$. Each
883 condition was performed on four (n=4) independent occasions. **(C)** Bright field images of CT29
884 organoids transfected with control (NT, siCTRL) or BCAM-silencing siRNA (siBCAM#1,
885 siBCAM#2) following 7 days of culture in regenerative Wnt+ media. Bars = 200μm. Bar graph to the
886 right shows area quantification of control and BCAM-silenced organoids. Median values are shown
887 and statistical analyses between groups were performed using ANOVA and two-tailed Tukey post-test;
888 significance $p < 0.05$. Each condition was performed on three (n=3) independent occasions. **(D)** Bar
889 graph shows proportions of small, medium, and large colonies in control- and BCAM-silenced CT29
890 organoids. Median values are shown and statistical analyses were performed using a 2way ANOVA,
891 multiple comparisons were controlled for using a Bonferroni post-test; significance $p < 0.05$. **(E)** Flow
892 cytometry plots showing EGFR and BCAM frequencies in control and BCAM-silenced CT27
893 organoids at day 3 of organoid culture in regenerative media. Bar graphs show median values of
894 $EGFR^{hi}$ and $EGFR^{lo}$ frequencies, and statistical analyses between groups were performed using
895 ANOVA and two-tailed Tukey post-test; significance $p < 0.05$. Each condition was performed on three
896 (n=3) independent occasions. **(F)** Bar graphs show frequency of cell G_1, G_2, and S cell cycle phases
897 measured by flow cytometry in control (NT, siCTRL) and BCAM-silenced (siBCAM#1, siBCAM#2)
898 CT29 organoids. Statistical analyses between groups were performed using ANOVA and two-tailed
899 Tukey post-test; significance $p < 0.05$. **(G)** IF images showing Brdu incorporation in control (siCTRL)
900 or BCAM-silenced day 7 organoids following 4 hr of BrdU pulse. Bar graphs show median values of
901 BrdU frequencies in each group. Bars = 200μm. Each condition was performed on three or four (n=3,
902 n=4) independent occasions. * = $p < 0.05$; ** = $p < 0.01$; **** = $p < 0.0001$.

Figure 5

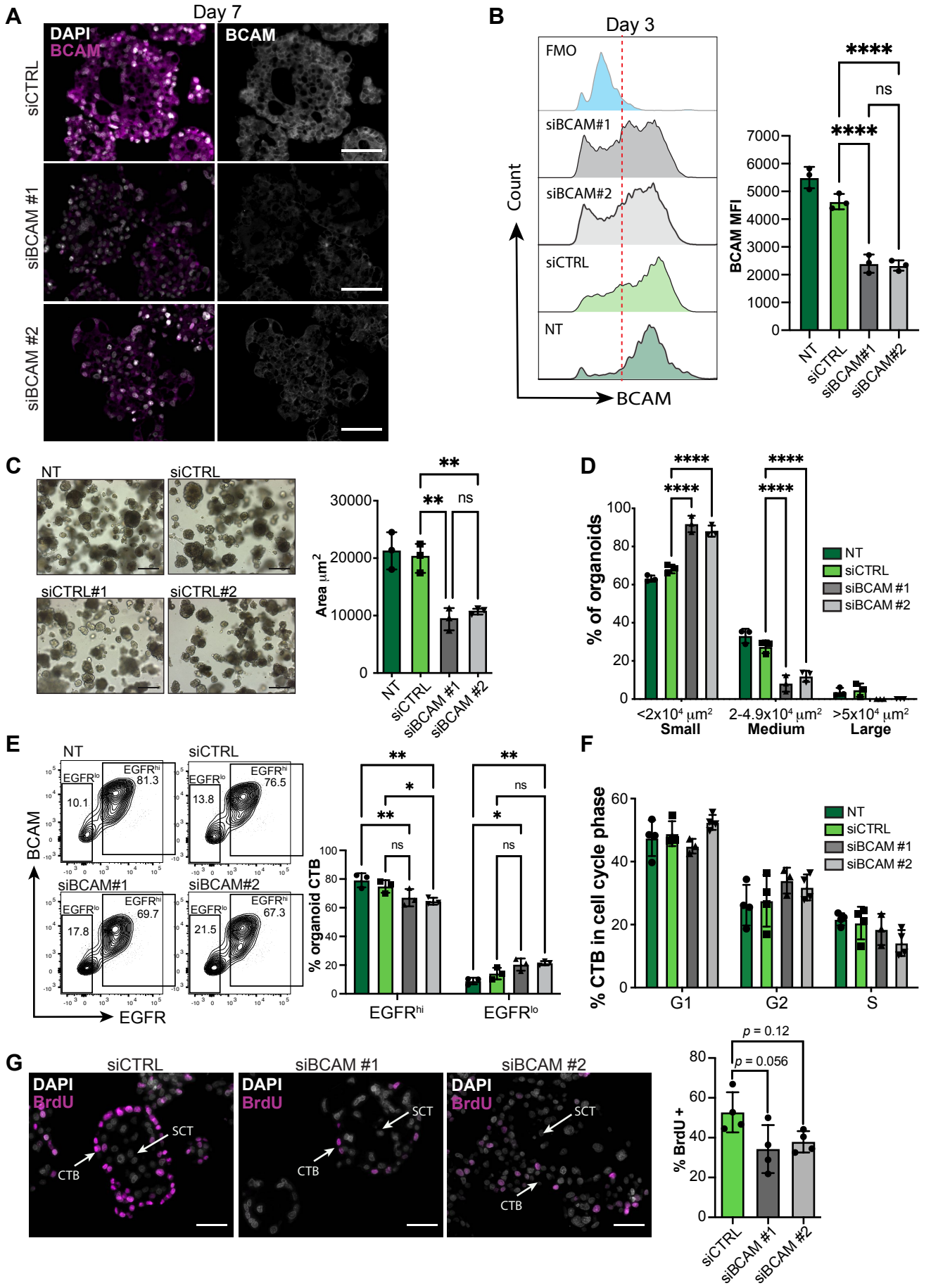
A
Day 7
DAPI
BCAM
BCAM
siCTRL
siBCAM #1
siBCAM #2
B
Day 3
FMO
siBCAM#1
siBCAM#2
siCTRL
NT
Count
BCAM
****
ns
****
BCAM MFI
7000
6000
5000
4000
3000
2000
1000
0
NT
siCTRL
siBCAM#1
siBCAM#2
C
NT
siCTRL
siCTRL#1
siCTRL#2
**
**
ns
Area µm²
30000
20000
10000
0
NT
siCTRL
siBCAM #1
siBCAM #2
D
****
****
****
****
% of organoids
100
80
60
40
20
0
NT
siCTRL
siBCAM #1
siBCAM #2
<2x10⁴ µm²
Small
2-4.9x10⁴ µm²
Medium
>5x10⁴ µm²
Large
E
NT
siCTRL
siBCAM#1
siBCAM#2
EGFRlo
EGFRhi
10.1
81.3
13.8
76.5
17.8
69.7
21.5
67.3
BCAM
EGFR
**
*
**
ns
**
ns
*
ns
% organoid CTB
100
80
60
40
20
0
EGFRhi
EGFRlo
F
% CTB in cell cycle phase
60
40
20
0
NT
siCTRL
siBCAM #1
siBCAM #2
G1
G2
S
G
siCTRL
siBCAM #1
siBCAM #2
DAPI
BrdU
SCT
CTB
p = 0.12
p = 0.056
% BrdU +
80
60
40
20
0
siCTRL
siBCAM #1
siBCAM #2

903 **Supplemental Figure 1: Sample quality control and single cell characterization of the first**
904 **trimester human maternal-fetal interface**
905 **(A)** Summary of workflow used for collection, processing, and single cell analysis of placental villous
906 cells. MFI, Maternal-Fetal Interface, 7AAD: 7-Aminoactinomycin D, FSC-A: Forward Scatter Area.
907 Violin plots showing the distribution of the raw number of **(B)** features, **(C)** the raw number of counts,
908 and **(D)** the percent mitochondrial DNA content remaining post quality control and data pre-processing
909 captured per cell during sequencing for each sample. Samples 1-6 (teal) represent the placental tissue
910 samples sequenced by the Beristain lab, samples 7-11 (red) represent the placental tissue samples
911 acquired from ArrayExpress, and samples 12-15 (grey) represent the decidual tissue samples acquired
912 from ArrayExpress. **(E)** Scatter plot showing the distribution of captured cells across principal
913 components 1 and 2 following dimensional reduction in principal component space. Cell positions are
914 calculated based on cell embeddings calculated during dimensional reduction by principal component
915 analysis. Cells are colour coordinated by source with teal representing those cells originating from
916 placental tissue samples sequenced in this study and red representing those cells originating from
917 placental and decidual tissue samples acquired from Vento-Tormo et al (ArrayExpress: E-MTAB-
918 6701). **(F)** UMAP plot of 50,790 captured cells, demonstrating 31 distinct clusters identified within the
919 first trimester human maternal fetal interface. Dashed lines separate maternal decidual immune cells
920 from non-immune cells and placental trophoblasts. Cells are colour coordinated by identity and
921 abbreviations are identical to those in Figure 1A. Epigland: epiglandular cell, fetal Endo: fetal
922 endothelial cell, dEndo: decidual endothelial cell, dSC: decidual stromal cell PV: perivascular cell,
923 pFib: placental fibroblast, Hb: fetal Hofbauer cell, M1: macrophage cell 1, M2: macrophage cell 2,
924 uNK: uterine natural killer cell. **(G)** UMAP projection of the captured maternal fetal interface cells,
925 stratified by gestational age. Early (left panel): 9803 early first trimester cells from each identified
926 cluster captured between 6-7 weeks gestational age, before the onset of maternal placental
927 vascularization. Late (right panel): 40,987 late first trimester cells from each identified cluster captured
928 between 9-12 weeks gestational age, after the onset of maternal placental vascularization. Cell cluster
929 names and colours correspond to those in Supplemental Figure 1E. **(H)** Heatmap showing the average
930 expression of known immune, non-immune, and trophoblast gene markers, as well as proliferation gene
931 markers in each identified cluster. Cell cluster names and colours correspond to those in Supplemental
932 Figure 1E. **(I)** Stacked bar plot showing the percent distribution of cells in each cluster with gene
933 signatures representing a cell in the gap 1 phase of proliferation, the gap 2 or mitotic phases of
934 proliferation, or the synthesis phase of proliferation. Cell cluster names and colours correspond to those

935 in Supplemental Figure 1E and abbreviations are identical to those in Figure 1F. **(J)** UMAP plots
936 showing gene expression in red of a mesenchymal cell gene marker (*VIM*), an immune cell gene
937 marker (*PTPRC*, encoding the CD45 protein), endothelial cell gene markers (*CD34* and *VCAM1*), and a
938 fibroblast gene marker (*ACTA2*). **(K)** UMAP plots showing gene expression in red of known
939 trophoblast gene markers used to subset and purify first trimester human trophoblasts from other cells
940 within the maternal fetal interface.
941
942 **Supplemental Figure 2: 3D-rendering of UMAP-informed trophoblast clusters**
943 Chorionic villi scRNA-seq clusters showing state-specific colors corresponding to CTB1-4, SCTp,
944 cCTB1, cCTB2, and EVT.
945
946 **Supplemental Figure 3: Monocle3 pseudotime quantification supports identification of CTB2 as**
947 **the progenitor origin**
948 **(A)** UMAP plot with constructed trajectory graph overlain. Cells are colour coordinated by relative
949 pseudotime value. **(B)** UMAP plot with constructed trajectory graph overlain. Cells are colour
950 coordinated by cluster identity. Cell cluster names and colours correspond to those in Figure 1C. **(C)**
951 UMAP plot highlighting the constructed trajectory graph which describes the path taken as CTB state 2
952 progresses into CTB state 3. Cells are colour coordinated by cluster. Cluster names and colours
953 correspond to those in Figure 1C.
954
955 **Supplemental Figure 4: 3D-rendering of UMAP-informed organoid trophoblast clusters**
956 Trophoblast organoid scRNA-seq clusters showing state-specific colors corresponding to CTB1-3,
957 SCTp, cCTB, EVT1, and EVT2.
958
959 **Supplemental Figure 5: Organoid colonies in BCAM^{hi} and BCAM^{lo} sorted organoids**
960 Bar graph shows the average of numbers of organoid colonies from BCAM^{hi} and BCAM^{lo} –sorted
961 CT29 organoids cultured over 11 days. Grey bars = BCAM^{lo}; Green bars = BCAM^{hi}.

Supplemental Figure 1

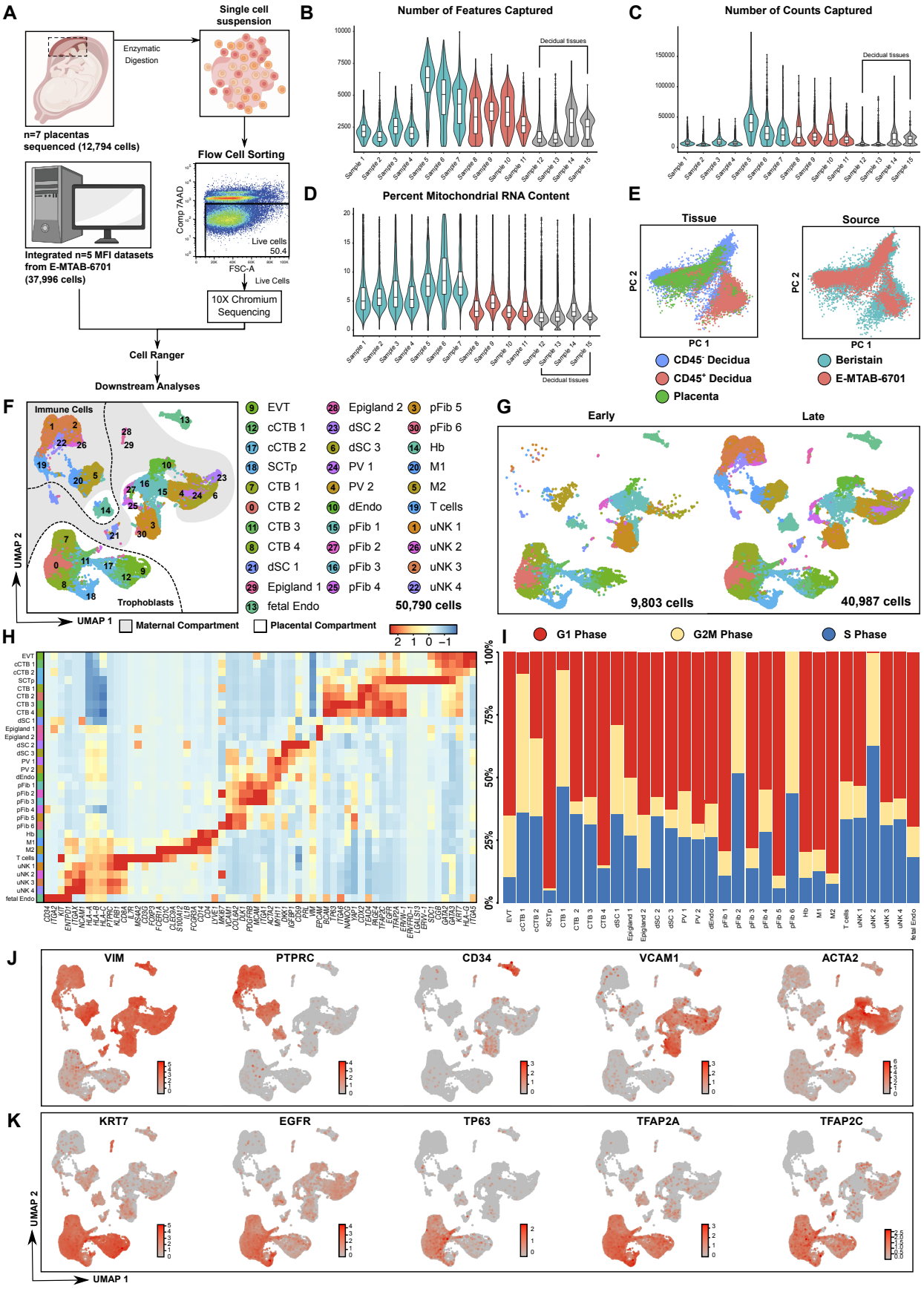

Supplemental Figure 3

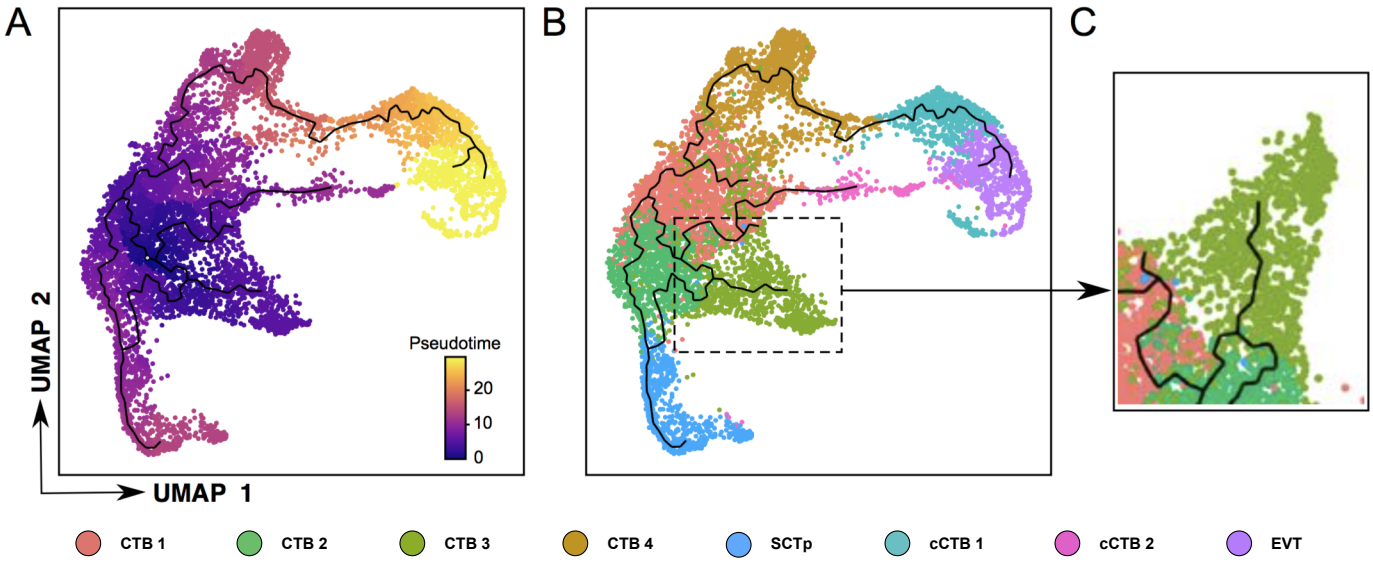
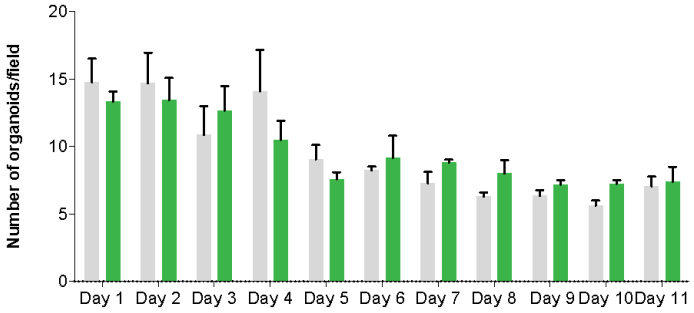
Supplemental Figure 5